Benha University
Faculty of Engineering Shoubra
Engineering Mathematics and
Physics Department

Nuclear Multi fragmentation and Particle Production Interactions of Heavy Ions in Emulsion nuclei

Thesis
Submitted to
Benha University - Faculty of Engineering Shoubra
In Partial Fulfillment of the Requirements for the Master Degree

In
Engineering Physics

By
Engineer
Abdelnasser Saber Abdelfatah Soliman
Demonstrator in Engineering Mathematics and Physics Department
Faculty of Engineering Shoubra, Benha University

Supervisor

Prof. Dr. A. Abdelsalam

Professor of Nuclear Physics
Physics Dept.
Faculty of Science
Cairo University

Prof. Dr. M. S. El-Nagdy

Professor of Nuclear Physics
Physics Dept.
Faculty of Science
Helwan University

Dr. A. M. Abdalla

Assist. Professor of Eng. Physics

Eng. Mathematics and Physics Dept.
Faculty of Engineering - Shoubra
Banha University

2012

وعلمك ما لم تكن تعلم وكان

فضل الله عليك عظيماً

صدق الله العظيم

(سورة النساء الآية ١١٣)

DEDICATION

To

My Father

(God rest his soul)

My Mother

And

My Wife

FORWARD

Forward

This work was carried out at Mohamed El-Nadi, High Energy Laboratory, Physics Department, Faculty of Science, Cairo University, Egypt.

ACKNOWLEDGEMENTS

Acknowledgment

First of all I would like to thank ***Allah*** *the most merciful and most graceful. Who without his guidance and inspiration nothing could have been accomplished.*

I'm extremely grateful to my advisor ***Prof. Dr. A. Abdelsalam****, Professor of Nuclear Physics, Faculty of Science, Cairo University, for suggesting the point of research , his continuous guidance, support and scientific supervision that enabled me to accomplish this study.*

I'm deeply grateful to my advisor ***Prof. Dr.*** **M. S. El-Nagdy,** *Professor of Nuclear Physics, Faculty of Science, Helwan University, for his continuous guidance, support and scientific supervision that enabled me to accomplish this study.*

I'm also grateful to my advisor ***Assist. Prof. Dr. A. M. Abdalla,*** Department *of Engineering Mathematics and Physics, Faculty of Engineering Shoubra, Benha University, for providing many facilities during experimental measurements, and scientific supervision that enabled me to accomplish this study.*

Most heartfelt thanks are to ***Assist. Prof. Dr. B. M. Badawy,*** *(Atomic Energy Authority), for his own great efforts in computer programs, continuous guidance, advice and support.*

Most heartfelt thanks are to ***Prof. Dr. Fatma Metawe,*** *for her own great efforts, continuous guidance, advice and encouragement.*

Most heartfelt thanks are to ***Dr. Hytham A.A.,*** *for his own great efforts, continuous guidance, advice and support.*

The author appreciates very much the continuous help of the staff members of Mohammed El-Nadi High Energy Laboratory, Physics Department, Faculty of Science, Cairo University, Giza, Egypt.

It is pleasure to acknowledge the help of the director and the staff of the Brookhaven National Laboratory (BNL) for providing us with the irradiated emulsion.

My sincere appreciation to all my colleagues' faculty of Engineering Shoubra, Benha University, for the unlimited support and encouragement, and to all whom contributed in the accomplishment of this study.

Finally special appreciation and greeting is to my parents, brothers, sisters and my wife. They do much effort for me in my whole life.

AIM OF WORK

Aim of the Present Work

The aim of this work is to study the inelastic interaction of ^{28}Si ions with emulsion nuclei at 14.6A GeV in order to obtain information about the factors which may affect on the different mechanisms responsible for producing grey and black particles in FHS and BHS. It is also aimed to investigate the source for the emission of grey and black particles. This is achieved through:

- Studying the characteristics of the multiplicity distributions of grey and black particles emitted from the interactions of ^{28}Si at 14.6A GeV with emulsion nuclei.

- Studying the angular distributions of the grey and black particles for the interaction of ^{28}Si with emulsion nuclei.

ABSTRACT

Abstract

This thesis is concerned with analyses of the fast, and slow hadrons production, in ^{28}Si -Em interactions at 14.6A GeV. The main motivation is the search for the effective mechanism responsible for this production. One key is the dependence of particle multiplicity on the projectile energy. In this species, ^{28}Si -Em interactions at 3.7A GeV is used for comparison.

The normalized multiplicity distributions of grey, black, and the heavily–ionizing particles are displayed at the two incident energies. The experimental results suggest that the incident energy is not an effective parameter in the target fragmentation system, regarding the limiting fragmentation hypothesis beyond 1 GeV.

The percentages of events accompanied by backward emitted grey and black particles tend to be constant, independently on the projectile size and energy. The experimental results suggest that these backward emitted particles are resulted from a decay system in a latter stage of the interaction. The main effective parameter in these particles production is the target size.

The multiplicities of the grey and black particles, emitted in both hemispheres, are correlated with the heavily–ionizing particles multiplicity, to form functions of target size. The system of grey and black particles emission in FHS is strongly correlated with that in BHS. This correlation is approximated in a linear relationship.

Basing on the modified Maxwell-Boltzmann distribution, the modified statistical thermodynamical model can describe the multiplicity and angular characteristics of the grey and black particles emission systems. The constancy in the anisotropy factors of these emission systems is utilized in the model modification to predict their velocities.

From the interactions of (p, ^{4}He**,** ^{6}Li, ^{7}Li**,** ^{12}C**,** ^{24}Mg**,** and ^{28}Si) with emulsion nuclei at (3.7 – 14.6A GeV), a constancy is observed in the average values of the emission angles for the grey and black particles. They are found to be $< \theta >_{g} \sim 64$ and $< \theta >_{b} \sim 80$, respectively.

CONTENTS

Chapter (I)
I. Theoretical Review on Experimental Results of nuclear collisions at High Energy

Chapter (II)

Experimental Techniques & Methods of Measurements

Chapter (III): Results and Discussions

LIST OF FIGURES

List of Figures

LIST OF TABLES

List of Tables

LIST OF SYMBOLS

The symbols used in this thesis are given below:

Physical quantity	Symbol
The Shrinkage factor of the emulsion.	(K)
The Grain density of the track.	(g)
The minimum value of the Grain density.	(g_o)
The Normalized Grain Density	(g^*)
The Linear Density of the Resolvable Clumps.	$(\underline{b})$
The Length between the Centers of two Grains.	(a)
The Average Value of the Length (a).	$\langle a \rangle = \xi$
The Lacunarity	(L)
The Dip Angle.	(α)
The Projection Angle.	(φ)
The Space Angle.	(θ)
The Cone Emission Angle.	$(\theta \leq 3^\circ)$
The Velocity of the Secondary Particles.	$(\beta = V/C)$
The Charge number.	(Z)
The Effective value of the Charge number.	$(Z_{eff.})$
The Charge number of the i^{th} emulsion nucleus	$(Z_{i.})$
The Mass number.	(A)
The Projectile Mass number.	(A_P)
The Target Mass number.	(A_T)
The Mass number of the i^{th} emulsion nucleus.	$(A_{i.})$
The Effective value of the Mass number.	$(A_{eff.})$
The Impact parameter.	(b)
The Radius of the Projectile nucleus.	(R_P)
The Target nucleus Radius.	(R_T)

List of Symbols

The Concentration of the $\mathbf{i^{th}}$ emulsion nucleus in Cm^3.	$(\mathbf{N_i})$
The Inelastic Reaction Cross section of the Projectile with the $\mathbf{i^{th}}$ type of the emulsion nuclei.	(σ_i)
The Total Inelastic Reaction Cross Section.	$(\sigma_{Inel.})$
The Experimental value of the Total Average Mean Free Paths.	$(\lambda_{exp.})$
The Theoretical value of the Total Average Mean Free Paths according to different models.	$(\lambda_{Cal.})$
The Different Cross Sections for the observation of a Particle momentum $\vec{q}$.	$\left(\frac{d^2\sigma}{d\vec{q}^2}\right)$
The Observed Particle Momentum.	$(\vec{q})$
The Incident Particle Momentum.	$(\vec{P})$
The Unobserved Particle Momentum.	$(\vec{P'})$
The Internal Momentum Distribution.	$(F(K))$
The Nucleon Rest Mass.	(M_n)
The Shower Particles Multiplicity.	n_S
The Average Value of the Shower particles Multiplicity	$\langle n_s \rangle$
The Average Value of the Forward Shower particles Multiplicity.	$\langle n_s^f \rangle$
The Average Value of the Backward Shower particles Multiplicity.	$\langle n_s^b \rangle$
The Grey particles Multiplicity.	(N_g)
The Average Value of the Grey particles Multiplicity.	$(< N_g >)$
The Normalized Multiplicity Distributions of the Grey particles.	$(P(N_g))$
The Average Value of the Forward Grey particles Multiplicity.	$(< N_g^f >)$
The Normalized Multiplicity Distributions of the Forward Grey particles.	$(P(N_g^f))$
The Average Value of the backward Grey particles Multiplicity.	$(< N_g^b >)$

List of Symbols

The Normalized Multiplicity Distributions of the Backward Grey particles.	$\left(\mathbf{P(N_g^b)}\right)$
The Forward to the Backward Ratio (anisotropy ratio).	$\left(\mathbf{F/B}\right)$
The Forward to Backward ratios for Grey particles productions.	$\left(\mathbf{(F/B)_g}\right)$
The Black particles Multiplicity.	$\left(\mathbf{N_b}\right)$
The Average Value of the Black particles Multiplicity.	$\left(\mathbf{< N_b >}\right)$
The Normalized Multiplicity Distributions of the Black particles.	$\left(\mathbf{P(N_b)}\right)$
The Average Value of the Forward Black particles Multiplicity.	$\left(\mathbf{< N_b^f >}\right)$
The Average Value of the Backward Black particles Multiplicity	$\left(\mathbf{< N_b^b >}\right)$
The Forward to the Backward Ratio of Black Particles (anisotropy ratio).	$\left(\mathbf{F/B}\right)_{\mathrm{b}}$
The Heavily ionizing particles multiplicity.	$\left(\mathbf{N_h}\right)$
The Average Value of the heavily ionizing particles Multiplicity.	$\left(\mathbf{< N_h >}\right)$
The Normalized Multiplicity Distributions of the heavily ionizing particles.	$(\mathrm{P}\ (\mathrm{N_h}))$
The predicted rational velocity.	χ_o
The Longitudinal Velocity of the Center of Mass.	β_{II}
The Characteristic Spectral Velocity of the Fragmentation System.	β_o
The Exponential Constant.	α_g^i, α_b^i
The Decay Constant.	λ_g^i, λ_b^i
Forward hemisphere	FHS
Backward hemisphere	BHS

INTRODUCTION

Introduction

In study of nucleon-nucleus and particularly nucleus-nucleus collisions, it is customary to divide the physics to be studied into different categories corresponding to impact parameter values. In violent collision region, the relatively large energy and momentum transfers manifest themselves in producing particles with large transverse momentum and/or in creating more particles in that collision [(1)]. Fragments from central collisions of relativistic heavy ions may originate from several qualitatively different subsystems of the overall decaying nuclear system, such as the fireball, the target spectators, or alternatively, an explosion of the fused target-projectile system [(2)]. Furthermore, the central collisions may be considered the most appropriate for studying the highly excited and compressed hadronic matter and the QGP [(3).] It is very important to learn as much as possible about all the phenomena which occur in interaction of high-energy nuclei. This should make easier the observation of the anticipated signatures of phase transition to QGP on the background of normal phenomena. Therefore, investigating the fragmentation is important in dealing with the reaction mechanism at each centrality region. The first experimental information about the fragmentation of nuclei was obtained in experiments with cosmic rays [(4)]. Knowledge of fragmentation characteristics of nuclei is required for solution of a number of problems of astrophysics, cosmic-ray physics, and radiation physics. In experiments (5, 6), the fragmentation was studied in the collision of (^{12}C, ^{16}O, ^{36}Ar, and ^{84}Kr) with emulsion nuclei at energy range (50-220A MeV). At these intermediate energies, there was no chance for pionization, as well as, the projectiles and target fragments were similar in the 4π space and limited in the shape of nuclear clusters. The selectivity of centrality degrees in such interactions was not enough on the basis of projectile or target fragments multiplicity. The fragmentation was directly proportional to the incident energy, i.e. the target and projectile fragments multiplicity increases with the incident energy. Hence, at that energy domain the limiting

fragmentation behavior can not be reached. Acceleration of nuclei to relativistic energies at Berkely and Dubna provided an opportunity to study this phenomenon in a systematic manner. Bevalac energy and Dubna energy (a few GeV/A) are special energies, at which the nuclear limiting fragmentation applies initially [7, 8]. The limiting fragmentation hypothesis implies that both target and projectile are fragmented independently of each other [9]. The projectile angular distribution showed that the limiting fragmentation hypothesis is valid for peripheral as well as quasi-peripheral collisions. The domain of validity of the limiting fragmentation hypothesis extends as the energy of the projectile nucleus increases. The energy independence of fragmentation cross sections had been indicated in Ref. (10) to hold at energies beyond the (1-2A GeV) region. At excitation energies comparable with the total binding energy~ 5-8 MeV/nucleon, the very existence of a long-lived compound nucleus becomes unlikely. In this situation the evaporation-like decay mechanisms should give way to an explosion like process leading to the total disintegration of the nucleus and the multiple emissions of nuclear fragments of different masses [11]. The fast process leading to the multi fragmentation final states was first discussed in Ref. (12) where the name "multifragmentation" was introduced. An active study of multifragmentation in reactions induced by relativistic protons and α-particles was continued in Dubna [13]. The high energy hadron-nucleus and nucleus-nucleus interactions are considered as a two stages process [14]. In the first stage, characterized by a time scale of the order of the light traversal time through the nucleus, multiparticle production takes place leaving the colliding nuclei in highly excited states. After a long time, the second stage, i.e. the de-excitation of the nuclear remnants starts, manifested by the emission of fragments. In target fragmentation, the target nuclei are usually found to completely disintegrate into light particles with $Z < 3$. The geometrical aspects of the fragmentation of nucleus can be understood in terms of the participant spectator model [15]. According to this model, at finite impact parameter, three regions are produced

after a collision between two nuclei. The participant region, the projectile spectator and the target spectator. The projectile spectator decays mainly into nuclear clusters since very little momentum transfer is required to form these fragments. The projectile fragments may thus be useful in determining the momentum distribution of a nuclear cluster inside the projectile nucleus. At relativistic energies, the separation in rapidity between projectile and target fragments is large ≥ 1 unit of rapidity. At such high energies, the target and projectile fragmentation regions are well separated in the rapidity. The physics of the two regions are believed to be similar. Consequently, no correlations exist between projectile and target nucleus and the modes of fragmentation are independent of target mass. The fragmentation cross sections can thus be factorized into a target and projectile related parts. In the context of many experiments at high energy, the distribution of target residues becomes approximately energy independent. The cross sections for a specific near target fragment produced in proton-or light-ion-induced reactions differ only by a constant factor that is close to the ratio of the total reaction cross sections [(16)]. The target fragmentation region is classified according to the emulsion nomenclature into two main groups of particles namely the black ($T_p \leq 26$ MeV for protons) and grey particles ($26 < T_p \leq 400$ MeV for protons), where T_p is the kinetic energy. The emission of the black particles has been well explained in terms of the statistical evaporation model [(17)], where complete thermalization is believed to occur in the final stages of reaction. Owing to the relatively high energy of the grey particles they are thought of as being liberated in the early stages of the reaction. In the present work the statistical model will be applied to the grey particles region as well as for the black particles, to examine its validity in both regions. The grey particle (fast hadrons) and black particle (slow hadrons), produced in relativistic heavy-ion reactions are a quantitative probe of the cascading processes in the spectator parts of the target nucleus [(18)]. On the other hand, in free nucleon–nucleon collision, the backward proton emission

($\theta_{lab} \geq 90°$) is strictly forbidden. Therefore, the production of such protons may reflect nuclear effects such as: the internal motion of nucleons inside the nucleus, short range correlation between nucleons or multiple nucleon–nucleon collision effects [19]. Therefore the study of the characteristics of the energetic protons emitted in the backward direction through the heavy ion collisions supplies effective information on nuclear effects [20]. In view of this, reported here is a detailed study on the production of protons (from the target) in forward and backward hemispheres, (FHS and BHS), in the interaction of ^{28}Si with emulsion nuclei at 14.6A GeV.

CHAPTER I

THEORETICAL REVIW OF NUCLEAR COLLISION AT HIGH ENRGY

Chapter I
Theoretical Review on Experimental Results Of Nuclear Collisions at High Energy

(I -1) Introduction

Since the half of the 20thcentury, the research in the field of elementary particle nuclear physics has been concerned with the nature of nuclear matter at /or near equilibrium. With the discovery of heavy nuclei in primary cosmic rays in 1948[(21)], studies of the nucleus-nucleus interaction at high energies became available. The recent availability of relativistic nuclear beams at several conventional accelerators around the world, makes it possible to study various aspects about nucleus-nucleus interactions at high energies and opens a new area of investigations in the field of research for relativistic nuclear physics[(22,23)]. Among these accelerators are, the Lawrence National Berkeley laboratory Bevalac, JINR Synchrophasatron at Dubna and RHIC at BNL. Recently, LHC at CERN permits a great opportunity to discover the new physics in hadron – hadron and nucleus – nucleus collisions in center of mass system.

The first experimental search for quark – gluon plasma in nuclear collisions was performed at the end of 1986 at CERN. The successful acceleration of oxygen (^{16}O) to 60 and 200 A GeV, as well as, sulfur (^{32}S) ions to 200A GeV at CERN SPS and ^{16}O beam to 14.6A GeV at Brookhaven opens up a totally new area in the field of heavy ion interaction.

(I - 2) Definitions
(I – 2.1) Target Separation:

Nuclear emulsion is a composite medium composed of H, CNO, and AgBr nuclei. It is a difficult task to separate interactions on different classes of targets. Although, there are many correlations between the measured parameters that give information regarding the target nuclei, it is impossible to find certain

separation criteria that give no admixture between those classes. Depending upon the target break–up, one uses the heavily ionizing particles multiplicity N_h as a parameter representing the impact parameter in experiment. Hence, the N_h – integral distribution method which is described explicitly in Ref. (24, 25) is used to select from the inelastic interactions samples of those with hydrogen H, light CNO, and heavy AgBr targets. According to this method, all events with $N_h > 8$ are considered to be due to interactions with AgBr group. The events with $N_h \leq 8$ are attributed to interactions with the H, CNO, and peripheral collisions with AgBr.

(I – 2.2) Impact Parameter:

The impact parameter, b of a nucleus – nucleus collision is classically defined by the distance between the straight line trajectories of the centers of the two nuclei before their interaction, as shown in Fig. (I-1a). the impact parameter is not directly measurable. It is thus necessary to find an observable strongly correlated with it. The multiplicity of heavily ionizing target fragments, N_h was used widely in nuclear emulsion experiments [26] for presenting their results. In an inelastic collision of a relativistic nucleus, not all the nucleons of the incident nucleus actually interact with the target nucleus. Some of the nucleons remain spectators or "stripping" nucleons, as they are frequently called. Fig. (I-1b) illustrates the fragmentation system of target and projectile in nucleus – nucleus collisions schematically. In interactions of nuclei heavier than the deuteron, the stripping particles may include not only nucleons but also larger fragments of the projectile nuclei in the form of stable and radioactive elements. The stripping particles lie in narrow momentum and angular intervals because of the Fermi motion of the nucleons in the projectile nucleus. All particles with $Z \geq 1$ and rapidity, (the Lorentz invariant parallel velocity), above half the beam rapidity, are regarded as projectile fragments of charge Z_{pf}. Therefore, in order to classify

the events with respect to the actual impact parameter, the parameter $Q = \sum Z_{pf}$, was introduced [27, 28].

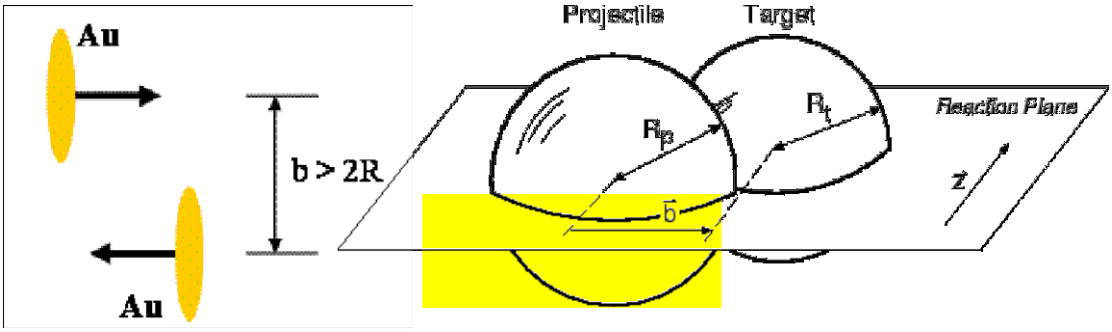

Fig. (I-1a): *A schematic presentation of the impact parameter.*

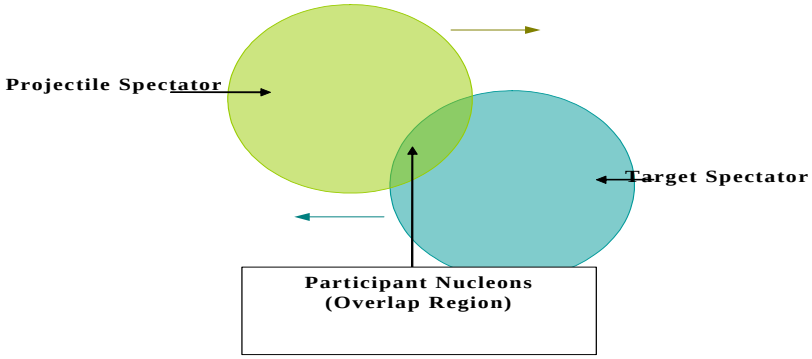

Fig. (I-1b): *A schematic diagram of the fragmentation system of target and projectile in nucleus – nucleus collisions.*

(I -3) Types of Relativistic Heavy Ion Collisions

In nucleus-nucleus collisions at high energies, there are various modes of interaction. The characteristic features of the interactions between nuclei at relativistic energies, from a geometrical concept, depend sensitively on the

impact parameter of the collision, which is the distance between the centers of the two nuclei as depicted in Figure (I -1a). This quantity characterizes the centrality of the collision. Ideally, only the nucleons in the overlapping zone, called fireball, participate in the collision as shown in Figure (I -2). The other nucleons are called spectators. So, according to the value of this parameter one can classify the relativistic heavy ion (RHI) interactions into peripheral, Quasi-central and central interaction.

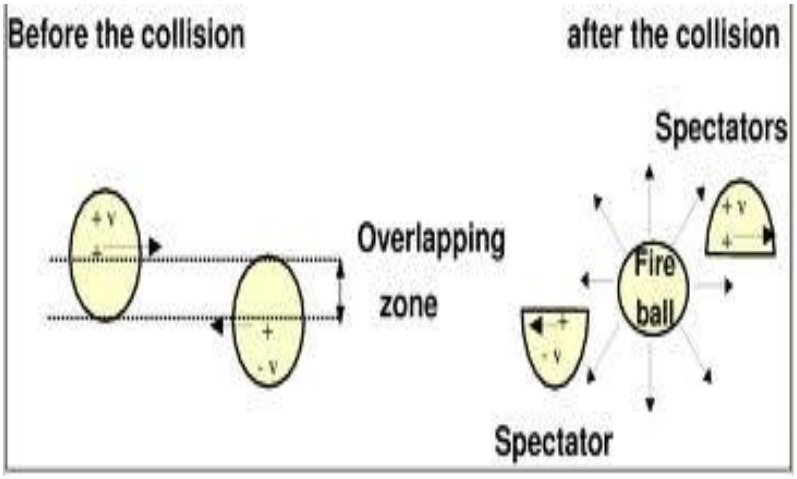

Fig. (I -2): *Definition of the impact parameter and fireball* [29].

In collisions involving impact parameters large enough as satisfies:

$$\mathbf{b > |R_T + R_P|}$$

Where $(\mathbf{R_T})$ and $(\mathbf{R_P})$ are "the target nucleus radius" and "the projectile nucleus radius" respectively, (b) is the impact parameter.

So that, no nuclear interactions occur, extremely strong electromagnetic fields are produced for a short time at the nucleus [30]. This process is called the electromagnetic dissociation (EMD) [31], which occurs when a virtual photon is exchanged between a target nucleus and the projectile.

(I -3.1) Peripheral Collision:

This kind of collision occurs when the impact parameter (b) between the colliding nuclei has value nearly equals to the summation of the radii (R_P and R_T) of the projectile and target nuclei, respectively i.e. $b \approx R_P + R_T$

In this type of collisions, the amount of momentum transfer through the overlap between the nuclei is small leading to the disintegration of the spectator part of the projectile nucleus through a fragmentation process. The projectile fragments (P.f's) are emitted in a narrow forward cone. The angular width of this cone is determined by the intrinsic Fermi–momentum distribution of the nucleons within the fragmented projectile nucleus [32, 33]. In the peripheral collision, the target nucleus also suffers fragmentation such that, the angular distribution of the fragments is isotropic.

(I-3.2) Quasi – Central Collision:

If the value of the impact parameter of the collision between two nuclei is ranging from the difference to the summation of the radii of these nuclei (i.e. $|R_P - R_T| \leq b < |R_P + R_T|$, such collision is referred to as a quasi–central and figure (I-3) shows that in this type of collision a partial overlap takes place between the projectile and target nuclei**.** In this case, some nucleons from both the projectile and target would participate in the collision [34, 35].

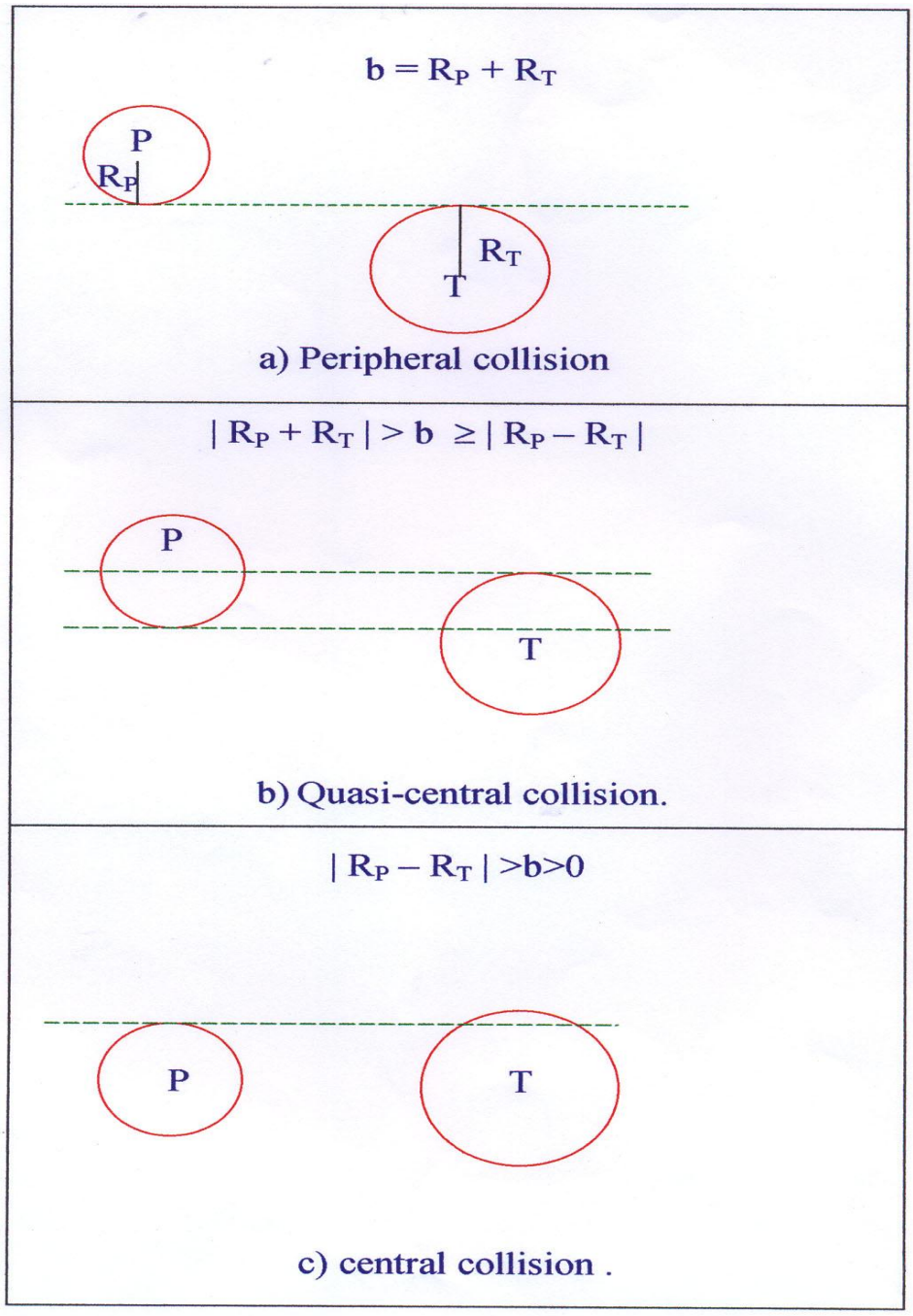

Fig. (I - 3): *The Types of the Interactions for Heavy Ions with Nuclear Emulsion at High Energy.*

(I -3.3) Central Collision:

In a collision of two nuclei, the impact parameter (b) can carry values from 0 to $R_P + R_T$, where R_P and R_T are the Radii of the two nuclei projectile and target respectively. When b = 0, it is called head-on collision, a complete overlapping of the projectile with target nuclear matter takes place, i.e. the two nuclei penetrate through each other. When collisions with $0 \leq b \leq (R_P + R_T)$ are allowed, it is called minimum-bias collision. In heavy-ion collisions, initial geometric quantities such as impact parameter and the collision geometry cannot be directly measured experimentally. Contrarily, it is however possible to relate the particle multiplicity, transverse energy, and the number of spectator nucleons (measured by a "zero-degree calorimeter" ZDC) to the centrality of the collisions. It is straight forward to assume that on the average,

1) The energy released in a collision is proportional to the number of nucleons participating in the collisions,

2) The particle multiplicity is proportional to the participating nucleon number.

Hence the particle multiplicity is proportional to the energy released in the collision. One can measure the particle multiplicity distribution or the transverse energy (E_T) distribution for minimum-bias collisions. Here the high values of particle multiplicity or E_T correspond to central collisions and lower values correspond to more Peripheral collisions. Hence the minimum-bias E_T or multiplicity distribution could be used for centrality determination in a collision experiment. Figure (I-4) shows the minimum-bias multiplicity (N_{ch}) distribution used for the selection of collision centrality. The minimum-bias yield has been cut into successive intervals starting from the maximum value of N_{ch}. The first 5% of the high N_{ch} events correspond to top 5% central collisions. The correlation of centrality and the impact parameter with the number of

participating nucleons has also been elaborated, in detail, by glauber-type monte carlo calculations employing woods–saxon nuclear density distributions[29].In emulsion, the charged particles emerging from the target nucleus are referred to as the heavily ionizing ones (h-particles). These h-particles include all charged fragments except the single-charged particles with $\beta \equiv (v/c) \geq 0.7$. This means that the h-particles consist of the grey (g) and the black (b) ones (which are to be defined later in subsections (II-7.2) and (II-7.3) respectively.

Usually, any reaction having h-particles more than (28) can be safely considered as being due to the most central collision with AgBr target nuclei. Although the processes of projectile and target fragmentation are identical in their respective rest frames, there are several distinctive features:

1) The region of projectile fragmentation is that region which is associated with the properties of the projectile.
2) The region of target fragmentation is that region which is associated with the properties of the target.
3) The mid-rapidity region is that region in which the characteristics of the particles produced from the interaction between the projectile and target nuclei are reflected.

Figure (I-4) shows how sensitively the characteristic features of heavy ion interactions at the relativistic energies depend on the impact parameter of collision. For illustration, the pseudorapidity parameter, η, ($\eta = - \ln \tan \theta/2$) is chosen since η is a suitable parameter and can be easily measured in emulsion (where θ is the emission angle in the laboratory frame). In this figure, P_f and T_f represent the projectile and target spectator fragments respectively. In addition, the important feature about the central collisions is the absence of the projectile fragments and both projectile and target nuclei are destroyed. In such type of interactions, high excitation levels are involved and large number of secondary fragments is emitted.

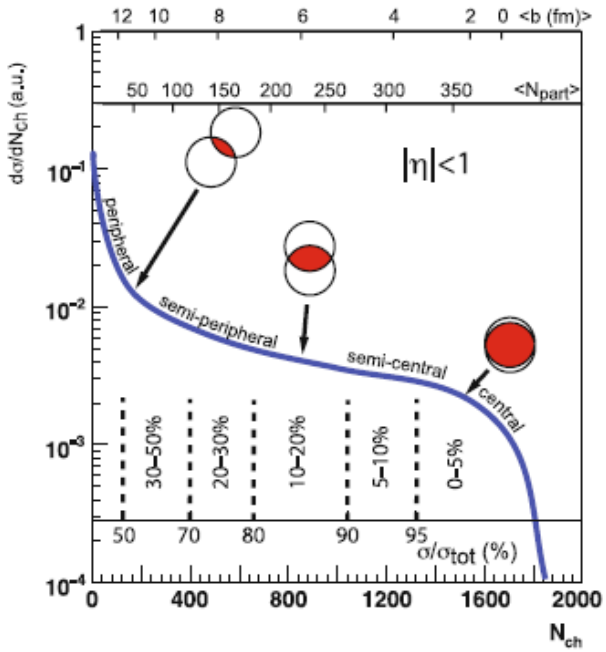

Fig.(I -4): *A cartoon showing the centrality definition from the final-state particle multiplicity and its correlation with the impact parameter (b) and the number of participating nucleons (N_{part}) in the collisions* [29].

(I - 4) Centrality Criteria

From straightforward geometrical considerations, central collisions are corresponding to the collisions with the impact parameters $0 \approx b \leq | R_T - R_{Proj} |$.

Exactly, there is no strict definition of what is meant by central collisions. To find the physical quantities that are sensitive to the centrality in nucleon – nucleus and nucleus – nucleus collisions at high energy, it is important to understand the behavior of the very hot and dense nuclear matter formed in these collisions. In some experiments the pion multiplicity was used to select central collisions. In other ones the centrality selection is based on the primary charged particle multiplicity N_{ch}. In experiments (36) the central

collisions of (^{12}C, ^{16}O, ^{36}Ar, and ^{84}Kr) with emulsion nuclei were studied at (50 – 220A MeV). At this range of intermediate energy, where no chance is found for pions to be created, the most central collisions were selected by momentum tensor elongation and multiplicity of target and projectile fragments.

Heckman et al [27] defined the more central collisions at Bevalac energy (relativistic energy), as interactions that exhibit an absence of projectile fragments i.e. Q = 0. Another approach of centrality estimation at high energy is based on the multiplicity of the target fragments N_h. This criterion is used in experiments (37, 38, 39, and 40). Although N_h and Q are used widely for selecting the central collision events, sometimes they are not adequate to execute the task. In hadron – nucleus (p – Em interactions) where the incident charge Z = 1, the criteria (Q = 0) can not be applied for selecting central events. Furthermore, N_h is applied for selecting central collisions with heavy targets (AgBr), while it can not be applied for selecting central events with light targets (H, CNO) where they are located in the low target fragmentation region at $N_h \leq 8$. Hence, it was argued that, the multiplicity of the backward shower particles, n_s^b is strongly correlated with N_h. This means that, the number of produced shower particles in backward hemispheres in each event (BHS) is a target dependent parameter. In some experiments, it showed also that, the dependence of backward hadrons emission on $n_s^b > 0$ is nearly equivalent to the dependence on Q = 0. In an experiment hold at Dubna by Abdelsalam et al [37] to study the central collisions of He and C with AgBr at 4.5A GeV/c, they selected the events at Q = 0. Also they showed that the events of central collision are characterized by $n_s^b \geq 1$. Thus, n_s^b can be used as an indication to the degree of violence of the collision and it can be introduced as a new centrality parameter associated with the target source achieving the violent interactions at its higher values ($n_s^b > 0$) [38,41,42].

(I- 5) Reactions Mean Free Path in Emulsion

The emulsion, being a composite target, is not equivalent to any single element for all processes. For each type of interactions it has an equivalent atomic number and atomic weight. The effective mass and charge numbers [(A_{eff}) and (Z_{eff}) respectively] of emulsion are given by[43]:

$$A_{eff} = \sum_i N_i \sigma_i A_i \; / \; \sum_i N_i \sigma_i \qquad \text{(I-1)}$$

and

$$Z_{eff} = \sum_i N_i \sigma_i Z_i \; / \; \sum_i N_i \sigma_i \qquad \text{(I-2)}$$

where (N_i), (A_i) and (Z_i) are the concentration in cubic centimeters, the atomic mass and the charge number of the i^{th} emulsion nucleus respectively. (σ_i) is the inelastic interaction cross–section of the projectile with this i^{th} type of emulsion nucleus.

If through out a total scanned lengths (L) of primary beam tracks, the number of resulted inelastic interactions (N), the average value of the experimental mean free path (λ_{exp}) are calculated according to the relation[25,26],

$$\lambda_{exp} = \frac{L}{N} \qquad \text{(I-3)}$$

(I- 6) Inelastic Interaction Cross Section

Glauber's multiple scattering theory [44, 45] has been used to predict nucleon–nucleus total cross–sections accurately in the few GeV range. The formalism involves the folding of the basic nucleon–nucleon scattering amplitudes with known nuclear matter distribution. The theory has been extended to nucleus–nucleus collisions [46] and used to predict the total inelastic cross–sections. The theory is essentially geometrical and the following proportionality is predicted from it,

$$\sigma_{\text{inel}} \propto (A_T^{1/3} + A_P^{1/3})^2$$

The best parameterization is given by [47],

$$\sigma_i = \pi r_o^2 [A_P^{1/3} + A_T^{1/3} - \beta (A_P^{-1/3} + A_T^{-1/3})]^2 \qquad \text{(I- 4)}$$

where $r_o = 1.32 \pm 0.01$ F and $\beta = 0.85 \pm 0.03$

On the other hand, the inelastic cross section is predicted empirically from a phenomenological "hard–sphere" model using "Bradt–Peters" formula [48]. For projectile nuclei at different incident energies up to 200A GeV, EMU01 collaboration[49] had deduced the cross section formula as,

$$\sigma_{PT} = 109.2(A_P^{0.29} + A_T^{0.29} - 1.39)^2 \text{ mb} \qquad \text{(I-5)}$$

Dubna experiments at 4.5A GeV/c, could formulate the inelastic cross section to be predicted as,

$$\sigma_{PT} = 10(1.46)^2 \pi (A_P^{(1/3)} + A_T^{(1/3)} - 1.21)^2 \text{ mb} \qquad \text{(I-6)}$$

For the formula (I-6), in the case of the proton–proton interactions, the cross–section will be [32.3 mb][49]. For the interaction of proton with any

nucleus of mass number A, as well as for the interaction of any projectile of mass number A with hydrogen target, the cross–section will be [$\sigma = 38.17\ A^{0.719}$ mb][49].

The total calculated inelastic cross–section is given by

$$\sigma_{inel.} = \sum_i N_i \ \sigma_i \ / \ \sum_i N_i \qquad \text{(I-7)}$$

The experimental cross sections belonging to each target group of interactions σ_H, σ_{CNO}, σ_{Em}, and σ_{AgBr} are computed as,

$$\sigma = \frac{1}{\lambda\rho} \qquad \text{(I-8)}$$

Here, λ is substituted as the measured mean free path of the projectile interactions with each target group and ρ is the density of that group of nuclei or the total number of the emulsion nuclei per unit volume of that group of nuclei, see table (II-1).

(I – 7) Production of Particles in the Backward Hemisphere

The majority of experiments on high energy nucleon–nucleus and nucleus–nucleus collisions were performed to study the characteristics of multiparticle production (mainly forward emission) which can in general, be described by the superposition models[50] in the momentum range of few GeV/c/nucleon. The phenomenon of backward particle emission in heavy ion reactions has attracted much attention from both the theoretical and experimental point of view [51]. Several publications have been introduced for the last four decades concerning the experiments which was done at Berkeley and JINR [52] and studied the production mechanism of hadrons in the backward hemisphere. Throughout, those studies of the backward particle emission (i.e. the particles emitted beyond the kinematics limit of those expected to be emitted from simple nucleon–nucleon collisions), it is preferable to review such production into the following categories:

a) <u>Proton production in the backward hemisphere:</u>

In free nucleon–nucleon collision, the backward proton emission is strictly forbidden. Therefore, the production of such protons may reflect nuclear effects such as: the internal motion of nucleons inside the nucleus, short range correlation between nucleons or multiple nucleon–nucleon collision effects[53]. Therefore the study of the characteristics of the energetic protons emitted in the backward direction through the heavy ion collisions supplies effective information on nuclear effects. In the incident energy range (E < 1 GeV per nucleon) Frankel has interpreted the data in terms of the quasi–two–body–scaling model [54], in which the primary mechanism for backward proton productions is a scattering between the incident nucleons and the target nucleons. They are the target nucleons, which are boosted onto the mass–shell and appear in the backward direction. Frankel was able to reproduce the low energy data by a simple structure function and suggested that this function was a measure of the internal momentum distribution of nucleons inside the target. The interpretation of this quasi–two–body scaling (QTBS) is based on different cross–sections for observing a particle of momentum $\vec{q}$, which obeys

$$d^2\sigma / d\vec{q} = C\, G\,(k_{min}) / \left| \vec{p} - \vec{q} \right| \qquad \text{(I – 9)}$$

In this equation Frankel originally treated C as a constant. The quantities $\vec{p}$ and $\vec{q}$ are the incident and observed particle momenta and G (k_{min}) is given by,

$$G\,(k_{min}) = \int F\,(k)\, k\, dk \qquad \text{(I – 10)}$$

The variable (k_{min}) is defined as,

$$k_{min} = \left| \vec{p} - \vec{q} \right| - \left| \vec{p}' \right| \qquad \text{(I – 11)}$$

F(k) is the internal momentum distribution of the target particle and $\vec{p}$ is the momentum of the unobserved particle. Both Frankel [54] and [Amado and Wloshyn] [55] have discussed the derivation of this expression. A more number of papers [56,57] have questioned the assumptions and interpretation of such data in terms of a simple–two– body reaction. Several experiments were done at Berkeley and JINR [58] for systematic study of the backward protons. The obtained data show that, the characteristic spectrum of the emitted protons with momentum above 400 MeV/c is independent of the projectile type and incident energy. All experimental data [59] about the backward proton characteristic above 2 GeV/nucleon gives an evidence for the limiting fragmentation hypothesis [60] which implies that, both projectile and target may be fragmented irrespective of each other. Fujita and Hüfner [61] suggested a model for backward proton emission mechanism which includes both initial correlations between nucleons in the target and final correlations between two nucleons. The final state interaction with the rest of the target nucleons (A – 2) is being neglected where A is the target mass number. Fujita [62] has extended this model to include multiple correlations. The improved model described well the data for the backward proton production at the incident energy less than 1 GeV. A theoretical work by [Frankfurt and Strikman][63] and [Yukawa and Furui][64] indicate that, the backward proton spectra induced by high–energy probes are mainly composed of spectator nucleons from the break up of correlated pairs in the nucleus. As such, these backward nucleons potentially reflected direct information of the nuclear wave function. Schroeder et al., [65] presented an experiment held at Berkeley [66] in order to obtain more information on the mechanisms responsible for high energy backward particle production by bombarding 2.1 GeV proton with various targets. At first, they found a large fraction of the events (≈ 50 percent) were found to have an associated negative track which

could be identified as a pion. Typically that pion appeared at $\theta_{lab} < 90°$. Thus, backward particles emission (typically the backward track is a proton) at 2.1 GeV is often accompanied by the production of a pion. They suggested that, the simple quasi–elastic process, NN $\rightarrow$ NN, as suggested by Frankel [67], was not the dominant mechanism, at that energy for, producing backward protons. Further information on possible reaction mechanisms can be obtained from a rapidity plot of the positively–charged particles (mostly protons) of those events. They state that "they appear to be evident for the role of pion production followed by absorption in the nuclear environment in the ejection of high–energy backward protons [68]. There were two possibilities:

1) Production of a pion followed by its absorption on two target nucleons resulting in two back-to-back nucleons, and

2) Production of the Δ^{++} (1232) and its subsequent absorption on a target nucleon via, $\Delta^{++} + N \rightarrow N + N$, resulting in the emission of two protons which would tend to have a near 180° correlation.

b) <u>Pion production in the backward hemisphere:</u>

A principal reason for studying the production of energetic pions from nuclei in the backward hemisphere through nucleon–nucleus and nucleus–nucleus interactions at high energies is that, in free nucleon–nucleon collision, such production is kinematically restricted. Observation of pions beyond this kinematic limit may be an evidence for exotic production mechanisms such as production from clusters [68]. The first experiment was performed at Dubna and Berkeley [69] on a systematic study of the energy dependence of charged pions produced at 180° in the collisions of

[0.8 – 4.89] GeV protons with nuclei. In Ref. (70) it was demonstrated that, from experiments using [5.14 and 7.52] GeV protons, Baldin et al.[71] observed a charged pion at 180° with energies up to four times larger than expected for free nucleon–nucleon collisions. They stated that, the dominant mechanism for producing such pions is on interaction between the incident proton and multinucleon clusters in the target nucleus, referring to this mechanism as "cumulative production".

Another experiment was presented by [Perdrisat, Frankel and Frati][72] using (0.6 GeV) protons. They observed pions at 155°, at energies beyond the nucleon–nucleon kinematic limit. However, they concluded that, the dominant mechanism is single scattering, where the incident proton interacted with a target nucleon producing the observed pion via the reaction

$NN \rightarrow NN\pi$.

In Ref. (73) the authors found an exponential energy spectrum for the pions, with a slope parameter $T_o \approx 60$ MeV, independent of the bombarding energy. Other experiment with 28.5 GeV protons [73] studying backward pion production from a tantalum plate located in the Brookhaven National Laboratory bubble chamber, yielded a slope of the energy spectrum consistent with the result of Ref.(71). The experiment given in Ref. (74) provides a definite test of a hard–scattering model [75] which was successful in explaining the scaling observed in forward pion production from nuclei at energies as low as 1 GeV. That model predicts that, the 180° spectra should be independent of energy, depending only on a scaling parameter [71]. An experiment was done at the Lawrence Berkeley Laboratory Bevatron [76] using extracted proton beams of (0.8, 1.05, 2.1, 3.5 and 4.89) GeV to study the pion production at 180°. The authors measured single–particle inclusive spectra of positive and negative pions produced at 180° in the collisions of protons with targets of C, Al, Cu, Sn and Pb at 3.5A GeV. Only

positive pions from Cu were measured. They first discussed the energy dependence of the slope parameter for charged pion production. Like the results of Baldin et al.[71] they found that the pion spectra fall off exponentially, and have therefore parameterized the Lorentz–invariant pion cross–sections by the form

$$E\, d\sigma / dP^3 = C\, e^{(-T/To)} \qquad (I - 12)$$

Where (T) is the pion laboratory kinetic energy. It was shown in Ref. (74) that, the dependence of (T_o) on the energy of the incident proton (T_p) for a Cu target only, is weakly dependent on target mass. The trend in the data was similar for both positive and negative pions. Using a combination of data for various backward pion production angles, Baldin reported [77] a similar trend and suggested that, it is related to the onset of limiting target fragmentation above $\approx 3 - 4$ GeV. The experimental dependence of (T_o) was compared with the predictions of the effective–target model [78] where the incident proton is assumed to interact in a collective fashion with the row of nucleons along its path. During the collision, this row was excited and in de–exciting emits pions in a fashion analogous to bremsstrahlung. Further experiments were performed to know more about the backward pions production behavior. On this way, the authors in Ref.(52) studied the results obtained from the experiments using nuclear emulsion, concluded that, the dependence of the backward emission of different particles on the projectile is weaker than that in the forward emission and also the backward emission tended to depend on the target size. In the same time they concluded that, the characteristics of particles emitted in the backward hemisphere are completely different from those emitted in the forward hemisphere. Therefore, the backward hemisphere is intimately connected with the target fragmentation region i.e. with that part of the phase space where all single particle characteristics are most safe from being dependent on the

projectile in accordance with the limiting fragmentation hypothesis when applied to nuclei [51]. Similar results are reached by the authors. [79, 80]

(I-8) Statistical Model

If the number of observed events is large enough, one can practically apply the statistical hypothesis of equal a prior probabilities in phase space. This allows to modify the Maxwellian distribution [27] for the momentum p of the emitted fragments (protons) which has the following form [with c = 1]:

$$d^2N / dPd\mu \propto P^2 \exp\left[-(P^2 - 2M\overline{\beta}_{ll}P_{\mu}) / P^2{}_o\right] \qquad \text{(I-13)}$$

Where $\overline{\beta}_{ll}$ is normally considered to be the longitudinal velocity of the particle-emitting system. $\mu = \cos\theta$, where θ is the laboratory angle between the momentum of the fragment of mass M and the momentum of the initial projectile, and $P_o = (2ME_o)^{1/2}$, where E_o is the characteristic energy per particle in the hypothetical moving system. We now examine how Equ. (I-13) would be modified when it is expressed in terms of range R and μ, the two quantities measured in experiment (27) .To good approximation, the R – β relation for Ilford emulsion is given by the power-low expression

$$\beta = k(RZ^2 / A)^n \qquad \text{(I-14)}$$

where k = 0.174, n = 0.29, R is in mm, and Z and A are the atomic and mass numbers of the fragment, respectively. In terms of β, Equ. (I-13) becomes

$$d^2N / d\beta d\mu \propto \beta^2 \exp[-(\beta^2 - 2\overline{\beta}_{II}\beta_{\mu}) / \overline{\beta}_o{}^2] \qquad \text{(I-15)}$$

where

$$\overline{\beta}_o = (2E_o / M)^{1/2} \qquad \text{(I-16)}$$

If this distribution is transformed to a distribution of track ranges R, the distribution in R- μ space becomes

$$d^2N / dRd\mu \propto (z^2 / A)^{3n} R^{3n-1} \times \exp[-(k^2R^{2n} - 2\beta_{II} kR^n \mu) / \beta^2{}_o] \quad \text{(I-17)}$$

where

$$\beta_{II} = \overline{\beta}_{II} (A / Z^2)^n \quad \text{(I-18a)}$$

and

$$\beta_o = \overline{\beta}_o (A / Z^2)^n \quad \text{(I-18b)}$$

It follows that the parameter denoted as

$$\chi_o = \beta_{II} / \beta_o = \overline{\beta}_{II} / \overline{\beta}_o \quad \text{(I-19)}$$

which is the ratio of the longitudinal velocity of the center of mass, β_{II}, to the characteristic spectral velocity, β_o, of the fragmenting system, is common to both the velocity and range spectra, and is independent of (A, Z).

Thus the longitudinal velocity β_{II} and spectral velocity β_o that characterize the range spectrum of unidentified fragments [equation. (I-17)] are related to the corresponding quantities for the velocity spectrum [equation. (I-16)] for any fragment (A, Z) by the factor $(A / Z^2)^n$, where n is the range-velocity index.

If $\beta^2 = \beta_L{}^2 + \beta_T{}^2$, where β_L and β_T are the longitudinal and transverse components of $\vec{\beta} = \vec{P} / M$ is introduced to Eq. (I-15), which then becomes factorable:

$$d^2N / \beta_T d\beta_T d\beta_L \propto \exp(-\beta_T{}^2 / \beta_o{}^2) \exp[-(\beta_L - \beta_{II})^2 / \beta_o{}^2] \quad \text{(I-20)}$$

Thus, the marginal probability distribution for β_L ($\approx$ rapidity y) is Gaussian, with

$$\langle \beta_L \rangle = \beta_{II} \quad \text{(I-21a)}$$

and

$$\sigma^2(\beta_L) = \beta_o{}^2 / 2 = E_o / M \quad \text{(I-21b)}$$

This variance can also be expressed in the form

$$\sigma^2(\tau) = \tau / M_n \qquad \text{(I-22)}$$

where the equivalent "temperature" of the system is τ (MeV/A) and M_n is the nucleon rest mass. The integration of equation (I-15) over the variables β and $\mu = \cos\theta$ leads to the following expression for N_{ij}, the expected number of fragments bounded by the ith interval of β, $\beta_i \le \beta \le \beta_{i+1}$ and the jth interval of μ, $\mu \le \mu \le \mu_{j+1}$:

$$N_{ij} \propto F(\mu_{j+1}) - F(\mu_j) + G(\mu_{j+1}) - G(\mu_j) \qquad \text{(I-23)}$$

Where

$$F(\mu) = [\exp(\chi_o{}^2\mu^2)]\{\exp[-\chi_o{}^2(\beta_i/\beta_{II} - \mu)^2] - \exp[-\chi_o{}^2(\beta_{i+1}/\beta_{II} - \mu)^2]\},$$

$$G(\mu) = \sqrt{\pi}\chi_o\mu[\exp(\chi_o{}^2\mu^2)\{erf[\chi_o(\beta_{i+1}/\beta_{II} - \mu)] - erf[\chi_o(\beta_i/\beta_{II} - \mu]\}$$

And $\chi_o = \beta_{II}/\beta_o$.

The angular distribution derived from equation (I-15) for fragments in ith interval $\beta_i \le \beta \le \beta_{i+1}$ is

$$\frac{dN}{d\mu} \propto [\exp(\chi_o{}^2\mu^2)] \times \{h(\beta_i) - h(\beta_{i+1}) - 2^{-1}\sqrt{\pi}(1 + 2\chi_o{}^2\mu^2) \times [g(\beta_i) - g(\beta_{i+1})]\} \qquad \text{(I-24)}$$

Where

$$h(\beta) = \chi_o(\beta/\beta_{II} + \mu)\exp[-\chi_o{}^2(\beta/\beta_{II} - \mu)^2]$$

And

$$g(\beta) = erf[\chi_o(\beta/\beta_{II} - \mu)]$$

When the angular distributions are measured without regard to fragment velocity, $dN/d\mu$ becomes a function of the single fitting parameter $\chi_o = \beta_{II}/\beta_o$ only. In this case, the ratio of the number of fragments in forward to backward hemispheres, F/B is given by

$$F/B = \frac{1 + erf\chi_o}{1 - erf\chi_o} \qquad \text{(I-25)}$$

To first order in χ_o, $\frac{dN}{d\mu}$ and F/B can be expressed as

$$dN / d\mu \approx \exp\left[\frac{4}{\sqrt{\pi}}\chi_o\mu\right], \qquad \text{(I-26a)}$$

$$F / B \approx \exp\left[\frac{4}{\sqrt{\pi}}\chi_o\right]. \qquad \text{(I-26b)}$$

Hence,

$$dN / d\mu \approx (F / B)^{\mu}, \qquad \text{(I-26c)}$$

$$dN / d\theta \approx \sin\theta (F / B)^{\cos\theta}. \qquad \text{(I-26d)}$$

For the values of F/B obtained in experiment (27), equation (I-26a) was a good approximation of the exact expression dN/dμ [equation. (I-24)].

CHAPTER II

EXPERIMENTAL TECHNIQUES & METHODS OF MEASUREMENS

Chapter II

Experimental Techniques & Methods of Measurements

(II – 1) Nuclear Track Emulsion

The nuclear emulsion is a very useful tool in experimental physics for investigating atomic and nuclear processes. The photographic emulsion consists of a large number of small crystals of silver halide embedded in gelatin. When charged particles pass through the emulsion, some of the halide grains are modified, but their modifications are invisible and this effect is described as the latent image formation. On immersing the nuclear emulsion plate in reducing bath, called the "developer", the latent images are turned into grains of silver. The latter, made up of finely divided crystalline aggregates, appear black within the transparent gelatin. The particles through the nuclear emulsion plate could therefore be seen under the microscope as trails of developed black grains. A true three–dimensional image of the particle trajectory is obtained. After processing the nuclear emulsion, it will occupy less volume than before and consequently its thickness will decrease. For any quantitative measurements of track densities, ranges and angles, it is necessary to know the exact original thickness of the emulsion layer at the time of the exposure divided by its thickness at the time of scanning. This ratio is called "the shrinkage factor (k)". The shrinkage factor may be different at different depths in emulsion. Also it may vary from place to place in a given plate. The nuclear emulsion has many advantages that make it a very useful tool than other types of detectors. These advantages are summarized in the following:

1) The emulsion can be used as a target as well as a detector for the study of the interactions with different target nuclei and of 4π–space of geometry.
2) It has the possibility of measuring energies and angles with high degree of resolution.

3) It can be used in studying the characteristics of new elementary particles and can detect the decay of the unstable neutral particles, rather than, its sensitivity to slow charged particles arising from the disintegration of the target nucleus.

4) Owing to the high stopping power of emulsion, a large fraction of short–lived particles are brought to rest in it before decay and hence their ranges and life times can be measured accurately.

According to the above mentioned advantages of the nuclear track emulsion, it seems that the nuclear emulsion method is a suitable technique for studying the interactions of high energy particles with nuclei in which many collisions occur with light nuclei like [carbon, nitrogen and oxygen] as well as heavy ones like [silver and bromine]. The less frequent interactions are the elementary collisions with the free hydrogen in the emulsion.

(II – 2) Details of the Used Emulsion Stacks:

In the present work, stacks of FUJI type of nuclear emulsion was exposed to the 14.6A GeV ^{28}Si beam at Brookhaven National Laboratory (BNL) Alternating Gradient in Synchrotron (AGS). Each emulsion pellicle of the stack has 600 μm thickness and 20 x 10 cm^2 dimensions. The chemical composition of FUJI type of nuclear emulsion is given in Table (II – 1).

This table also gives the number of atoms per cm^3 corresponding to each element of the emulsion constituent.

Table (II– 1): *The chemical composition of FUJI Track Nuclear emulsion.*

Element	Charge Number	Mass Number	Number of Atoms/cm^3 x 10^{22}
H	1	1	3.2093
C	6	12	1.3799
N	7	14	0.3154
O	8	16	0.9462
S	16	32	0.0134
Br	35	80	1.0034
Ag	47	108	1.0093
I	53	131	0.0055

(II – 3) Irradiation of the Stack

There are two types of the irradiation of the nuclear emulsion; the first type is the parallel irradiation in which the beam is parallel to the length of the stack, the second type is the perpendicular irradiation in which the beam is perpendicular to the X-Y plane of the stack, as shown in figure (II-1). The type used in the present work is the parallel irradiation.

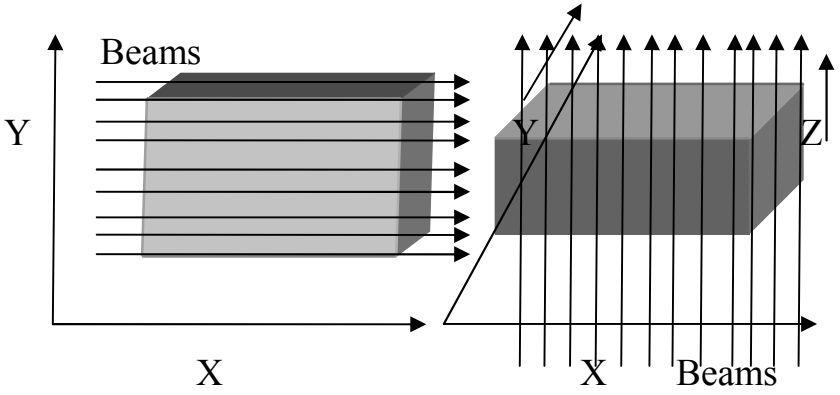

Fig. (II-1): *Parallel Irradiation and Perpendicular Irradiation.*

(II – 4) Microscope Description

In the present investigation two types of microscopes were used, one in the scanning and the other in the measuring respectively:

(II – 4.1) The scanning microscope:

The scanning of the emulsion pellicles was carried out using 850050 STEINDORFF German microscopes. It has a stage of $18\times16cm^2$ with an opening $7\times2.5cm^2$. Stag adjustment in the X-direction is possible over a total length 7.8 cm with reading accuracy of the order of 0.1 mm. oil immersion objective lens with magnification 100X was used for scanning the emulsion plates. Each primary track was picked up at the penetrating edge of the pellicle and was carefully forward until it either interacted or escaped from the pellicles.

Fig. (II-2): *850050 STEINDORFF German microscopes.*

(II – 4.2) The measuring microscope

In the present experiment, the Russian microscope type (MSU–9) was used for measurements. It has a rotatable metal stage which can rotate 360 degree about the optical axis of the microscope. The motion of this stage in the X-direction is read to 20μ with an accuracy of nearly 5μ. The stage can be moved either continuously or in adjustable fixed steps (cell length) of 100, 200 or 500μ. In the Y-direction the motion can be measured using a scale attached to one of the binocular eyepieces. This scale can be easily calibrated such that each division is corresponding to 16.6 μ with an accuracy of about 0.1 μm for objective lens and eyepiece of magnification 60x and 15x respectively. The eyepiece has a cross wire which helps in a lot of measurements. As for Z direction, the motion is read on a drum of one scale division equals to 1μ. Rough estimates to 0.5 μm can be easily made. The Russian microscope contains a rotatable geniometer, of 360º measuring range with a reading accuracy of 0.1º.

The objective lenses used are:

1. 15x Binocular eyepiece.
2. Dry lenses with 10x and 40x magnification.
3. Oil immersion lenses with 60x and 90x magnification.

Fig. (II-3): *The Russian Microscope type (MSU-9).*

(II -5)The Scanning Techniques [81, 82]

The reaching of the balance between the efficiency and the procedure to locate the events in the nuclear emulsion plates is called the scanning techniques.Generally; the following two possible types of the scanning techniques could be performed.

1) The Area Scanning.
2) The Along the Track Scanning.

(II-5.1) The Area Scanning:

The area scanning of the pellicle is usually used for the Events located in the nuclear emulsion volume; this is done by scanning field of view followed by

field of view in strip wise position. Each field of view is scanned throughout its depth, for high efficiency the field of view must be divided in to numbers of sufficiently small separated areas.

This type of scanning is useful in the cosmic rays work, where the primary particles enter over a wide range of solid angles or in the case of decays of neutral particles or when searching for certain type of interaction. The principle disadvantage of this technique is the possible failure of detecting the small events particularly events with N_h=0, 1 and $n_s \leq 4$ (where N_h is the heavily ionizing particles multiplicity while n_s is the shower particles multiplicity).

(II-5.2)<u>The Along the Track Scanning</u>:

This type of scanning is used when the trajectories of the incident particles are almost in the plane of the nuclear emulsion; the along the track scanning is the most useful technique to locate all different kinds of events. In this method, every track of the incident particles is followed along its length; until it interacts or leaves the pellicle, the location of each interaction of the incident projectile nuclei in the nuclear emulsion plates was registered in the scanning scheme with the aid of special squares on each plate (each square characterized by four numbers). In the present work, the along the track scanning is performed twice, where it is fast in the forward direction and slow in the backward direction; to be sure that the Recorded Events didn't include interactions from the secondary Tracks of the other interactions. Since the trajectories of the incident particles are almost in the plane of the nuclear emulsion; the nuclear track is adjusted to be parallel to the motion of the stage. This kind of fast scanning can only be applied at high energies when multiple coulomb scattering becomes small.

(II -6)The Grain Density and the Specific Ionization

When the charged particle is passing through the photographic nuclear emulsion; it will slow down via losing its kinetic energy; due to its inelastic interactions with the nuclear emulsion atoms along its path. The charged particle loses its kinetic energy; via the ionizations of the grains of silver halides and also via multiple elastic and inelastic scattering, which leading to trails of ionized silver halides along its path. The grain density is defined as the number of developed grains of silver halides per unit path length of the particle's track. It is denoted by (g) in a track corresponding to a particular value of specific ionization of such particle, so obviously it depends on some factors such as the degree of the development of the nuclear emulsion, the velocity and the charge of the ionizing particle. In order to obtain high accurate results, it is essential to determine the normalized grain density (g^*)

$$g^* = g / g_o \qquad \text{(II-1)}$$

Where (g) is the observed grain density per 100 μm for the emitted secondary particles after performing the dip angle correction. And (g_o) is the grain density per 100 μm of the energy relativistic track of minimum ionization i.e. singly charged particle or electron, both values of (g, g_o) is counted in the same plateau region and at the same depth in the nuclear emulsion. The most suitable method to measure the grain density is to count their number in a certain length of the choosing track, at low values of it; the error in the measurements mayn't be large, i.e. neglected. But obviously, as soon as the grain density increases in value; it becomes very impossible to counting them in the clump; so one must determine the linear density (b) of the resolvable clumps which has known as the blobs which is consisting of one or more developed grains. Suppose that (a) is the length between the centers of two grains and so by

denoting $\langle a \rangle = \zeta$; then the blob density is related to the grain density by equation.

$$\underline{b} = g e^{-\zeta g} = g \Big/ \left(e^{\zeta g} - 1\right) \qquad \text{(II-2)}$$

This method is equivalent to determine the gap density in the choosing track and counting of gaps may be preferable when the grain density is high in value.

$$L = e^{-g\xi} = \frac{\text{Total gap Length measured}}{\text{Total track Length measured}} \qquad \text{(II-3)}$$

So, by measuring the lacunarity (L) one can estimate the grain density as shown in equations. It is of great importance to deduce the specific ionization from the characteristic of the track. Since, the specific ionization is defined as the probability that at the passage of the ionizing particle through silver halides grains; so they will be developed. Consequently, as we confirmed previously the value of the specific ionization i.e. this probability is dependent on the energy dissipated in the silver halides grains; so obviously, the specific ionization is function of the particle's specific energy loss. In the present work (g_o) the grain density per 100 μm of the high energy relativistic track of minimum ionization i.e. singly charged particle or electron is 30 grains per 100μm, which is the average over different emulsion plates.

(II -7)The Classification of the Secondary Charged Particles

The classification of the secondary charged particles according to the blob density was first suggested by H. Camerini. et al.When the fast high energy particles collide with the emulsion nuclei; the tracks of the secondary charged particles are produced which are classified into three types according to the normalized grain density (g^*) which is given by the equation (II-1). Figure (II-4) shows a picture of the interaction between the projectile and the target in the nuclear emulsion and secondary particles resulting from the interaction in the form of track.

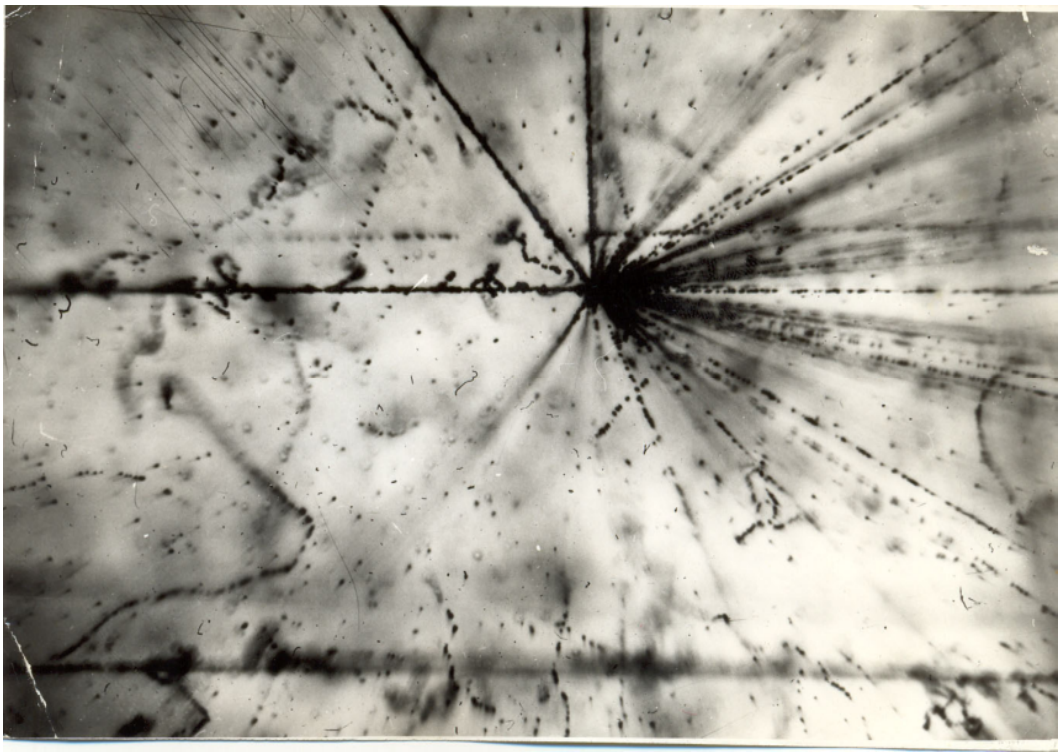

Fig. (II-4): *Photographic picture of an inelastic interaction (star) observed in nuclear emulsion as viewed by microscope.*

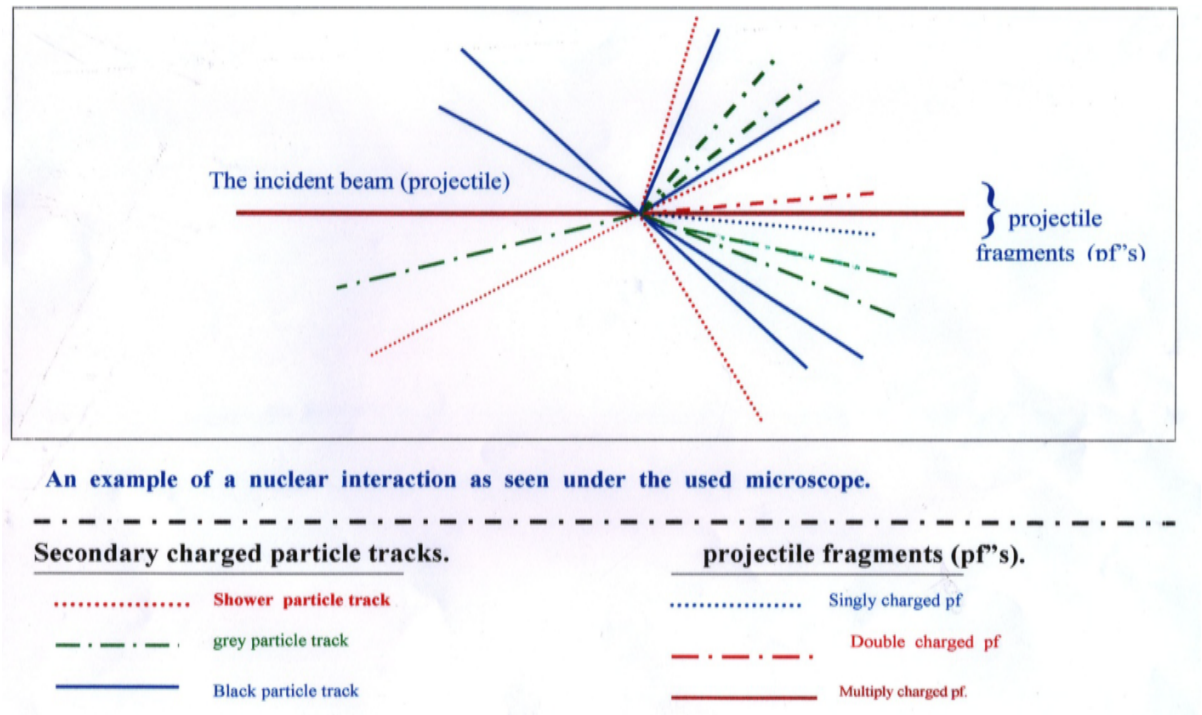

Fig. (II-5): *A schematic diagram of a star as seen under used microscope.*

(II-7.1) The Shower Tracks:

The shower tracks are characterized by the value of the normalized grain density ($g^* \leq 1.4$) and very high value of the velocity ($\beta = v/c \geq 0.7$).The shower tracks having emission angle ($\theta \leq 3^o$); are subjected to multiple scattering measurements for the momentum determination in order to separate the produced "Pions" from the singly charged projectile fragments. Most of the shower particles are mesons with energy (E > 50 MeV) contaminated with small fraction of fast protons with energy (E > 400MeV), charged K-mesons, antiprotons and hyperons. The shower particles multiplicity is denoted by (n_s), which its value gives good estimates of the number of the charged π-mesons produced in the interaction. The kinetic energy of some shower tracks is given in table (II-2).

(II-7.2) The Grey Tracks:

The grey tracks are characterized by the value of the normalized grain density ($1.4 < g^* \leq 10$), the value of the velocity ($0.3 < \beta < 0.7$), where most of them are recoil protons having range in the nuclear emulsion (L > 3000μm), which correspond to proton energies in the range from 26MeV up to 400 MeV. Some of the grey tracks may be due to emitted deuterons, tritons, helium nuclei and nearly about (5%) due to slow π-mesons. The grey tracks multiplicity is denoted by (N_g). The kinetic energy of some grey tracks is given in table (II-2).

(II-7.3) The Black Tracks:

The black tracks are characterized by the value of the normalized grain density$\left(g^* \geq 10\right)$, the value of the velocity ($\beta \leq 0.3$), where most of them are due to protons having "Range" in the nuclear emulsion (L ≤ 3000), which correspond to proton energies (E < 26MeV). The black tracks may be also due to deuterons, α-particles and heavy fragments. The black tracks multiplicity is denoted by (N_b). The kinetic energy of some black tracks is given in table (II-2).

The grey tracks and the black tracks are known as tracks of the heavily ionizing particles with the value of the velocity ($\beta < 0.7$). The heavily ionizing particles multiplicity is denoted by (N_h).

$$N_h = N_g + N_b \qquad \text{(II-4)}$$

Table (II-2): *The classification of particles according to their kinetic energy in MeV.*

Particle	Shower Track Particles	Grey Track Particles	Black Track Particles
π	K.E.$\geq$ 60	12 < K.E. < 60	K.E. $\leq$ 12
K	K.E.$\geq$ 212	20 < K.E.< 212	K.E. $\leq$ 20
^1H	K.E.$\geq$ 400	26 < K.E. < 400	K.E. $\leq$ 26
^2H	K.E.$\geq$ 800	36 < K.E. < 800	K.E. $\leq$ 36
^4He	K.E.$\geq$ 1600	105 < K.E. < 1600	K.E. $\leq$ 105

Table (II-3): *Parameters for classification of protons into shower track, grey track and black track.*

Type of Track	(g^*)	Range	K.E. (T) (MeV)	$\beta = v/c$
Shower	$g^* \leq 1.4$	---------	$T \geq 400$	≥ 0.7
Grey	$g^* \geq 1.4$	$(L > 3mm)$	$26 \leq T \leq 400$	$0.3 < \beta < 0.7$
Black	$g^* \geq 10$	$(L \leq 3mm)$	$T \leq 26$	≤ 0.3

(II - 8) Identification of Relativistic projectile fragments

The relativistic projectile fragments PF's are produced from the incident beam during its interaction with the emulsion nuclei , with emission angles (in the forward direction) depend on the projectile energy and have the following criteria :

1) $g/g_o < 1.4$ for Z = 1 RPF's
2) $g/g_o \sim 4$ (with no change of ionization when followed up to a distance of at least 2cm from the interaction center) for Z = 2 RPF's
3) $g/g_o > 6$ (with no change of ionization when followed up to a distance of ~ 1 cm from the interaction center) for $Z \geq 3$ RPF's

The charge identification of relativistic fragments of charge Z=1 was made by measuring the grain density g, for the shower tracks in the forward direction and which fulfilled the criterion (1). There are two methods to identify the Relativistic projectile fragments, will be discussed in the following,

(II– 8.1) Gap Density Method:

The charge identification of relativistic fragments of $(Z \geq 2)$ was made by measuring the gap density along the track which is associated with the energy loss. Consequently one has taken the energy loss of charged restricted to the track core (REL) as the theoretical counter part of the measured parameter. One has therefore assumed that, electrons with a kinetic energy above 2 Kev do not contribute to the blackness of the track. Thus, to identify the charge of a relativistic fragments, using this method, one measures the frequency of with a length > 2 μm at the star and in at least one point more than 2 cm from the star. Thus by counting the number of gaps of any two track and knowing the charge of one, the charge of the other can be determined from the inverse proportionality gaps with charge.

(II– 8.2) Delta-Ray Method:

A charged particle while passing through a material medium interacts with it as atomic interactions. As result of which, some electrons are knocked out .In sensitive nuclear emulsion these electrons produce short thin tracks projecting from the trajectory of the parent particles. These ejected electrons from the atoms which have the ability to ionize other atoms are known as delta rays .The production of these rays depend on the charge and velocity of the particle.

For a projectile of charge Z and velocity v, the δ-ray density is given by

$$N_{\delta} = Const.Z^{2}/\beta^{2}\,(1/W_{\min} - 1/W_{\max})$$

Where β = v/c , W_{max} is the maximum energy transferred to knock on electron and W_{min} is the minimum energy required to produce a visible δ-ray W_{max} increases as the velocity of the projectile increases ,

And consequently we have:

1) For non relativistic particles both $1/\beta^2$ and $1/W_{max}$ terms increase as v decreases, this makes the N_{δ} goes through a maximum value at a certain value of β.
2) At relativistic velocities, $1/\beta^2$ and $1/W_{max}$ become small and consequently N_{δ} reach a plateau value.

For velocities of the same order of magnitude, the maximum values of densities $N_{\delta 1}$ and $N_{\delta 2}$ produced by two particles of charges Z_1 and Z_2 respectively over residual ranges are connected by the relation:

$$N_{\delta 1}/N_{\delta 2} = Z_1^2/Z_2^2$$

The complex appearance of δ-ray, however, makes it very difficult to establish a reliable set of counting criteria that would ensure perfectly uniform

and reproducible observations. In this work, the measurements of projectile fragments were greatly simplified by the persistence of relativistic beam criterion i.e. counting δ-ray with a different numbers of ''grain''velocity. The grains was employed and also we counted δ-ray over a track segment of 10 mm from the center of the interactions. These measurements were confined to a depth between 30 μm and 220 μm from the surface of the emulsion, and a distance of at least 3 mm from the edges. Under these conditions the corrections due to the variation of the degree of development of the plates can be neglected.

(II -9)The Angles Measurements

(II-9.1) The Emitted Secondaries Geometrical Relations:

Assuming that the primary beam moving in the $\overrightarrow{XO}$ direction interacts with a particle or a nucleus at the point (A) and produces the secondary particle track $\overrightarrow{AB}$ as shown in figure (II-6).Where the dip angle (α) is defined as the angle included between the secondary particle track $\overrightarrow{AB}$ and its projection in the nuclear emulsion plane (XOY) plane i.e. $\overrightarrow{AC}$ .While the projection angle (φ) of the secondary particle track is defined as the angle included between the direction of the Primary Beam $\overrightarrow{XO}$ and the projection of the secondary particle track $\overrightarrow{AB}$ in the nuclear emulsion plane (XOY) plane i.e. $\overrightarrow{AC}$. The space angle (θ) is defined as the angle included between the secondary particle track $\overrightarrow{AB}$ and the direction of the primary beam $\overrightarrow{XO}$.

$$\begin{aligned} \cos\varphi &= OA/AC \\ \cos\alpha &= AC/AB \\ \cos\theta &= OA/AB \\ \cos\theta &= \cos\varphi\cos\alpha \end{aligned} \qquad \text{(II-5)}$$

If the primary beam with the dip angle(α), is adjusted to be parallel to the X-direction of the microscope, then the space angle (θ) will have the form.

$$\cos\theta = \cos\varphi\cos(\alpha \mp \alpha_{\circ}) \qquad \text{(II-6)}$$

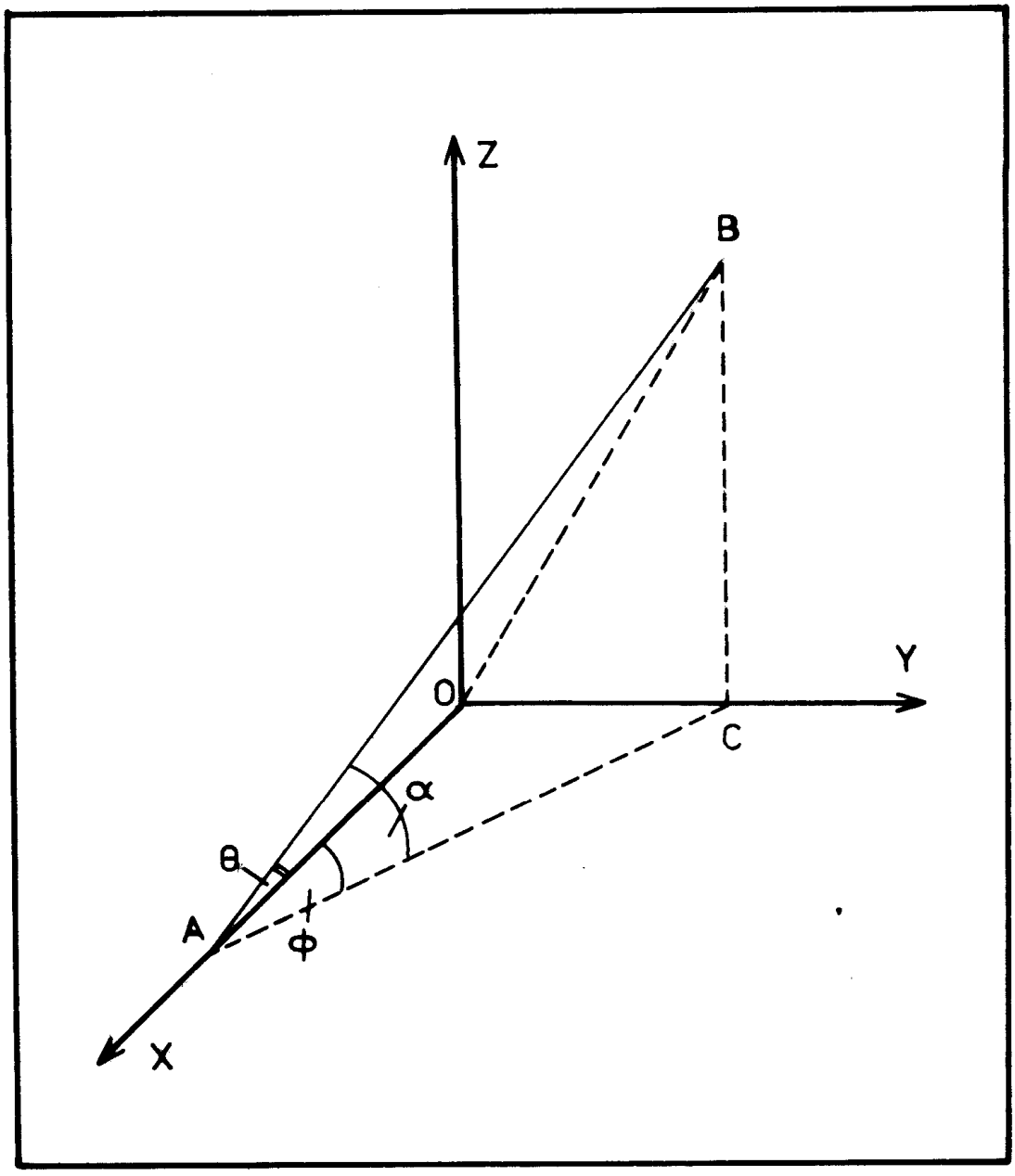

Fig. (II-6): *The geometrical representation for the beam and the Secondary Particle track.*

(II-9.2) <u>The Projection Angle Measurement</u>:

Measuring the projection angle (φ) of the secondary particle track is performed through the following steps. When $(\varphi \geq 1^{\circ})$.

1) The nuclear emulsion plate should be placed and fixed on the metal stage of the microscope.
2) The center of the interaction (A) should be adjusted; so as to be coincided with the center of the field of view.
3) Using the Rotatable Metal Stage of the microscope, "the Primary Beam" should be adjusted; so as to be parallel to the X-direction of the microscope.
4) The cross wire of the eyepiece is rotated to be coincided with each of the secondary particle track separately.
5) Then taken the reading directly from the geniometer within accuracy of 0.02° using The KSM1 nuclear track measuring microscope, while using the Russian microscope type (MSU9)" the accuracy become 0.1°.

When $(\varphi < 1^{\circ})$; the projection angle (φ) of the secondary particle track is measured using the coordinate's method of the following steps.

1) The metal stage of the microscope is moved a distance (X) microns along the forward direction of the primary beam $\overrightarrow{XO}$.
2) Determination the (Y) position at both of (A) at the center of the interaction and at the moving distance (X); so (ΔY) is evaluated.
3) Notice that the projection angle (φ) of the secondary particle track is ranging from 0° to ±180° and it is calculated by using the equation.

$$\varphi = \tan^{-1}\left(\Delta Y / X\right) \qquad \text{(II-7)}$$

(II-9.3) <u>The Space Angle Measurement</u>:

Measuring the space angle (θ) of the secondary particle track is performed through the following steps.

1) The nuclear emulsion plate should be placed and fixed on the metal stage of the microscope.

2) The center of the interaction (A) should be adjusted; so as to be coincided with the center of the field of view.

3) Using the rotatable metal stage of the microscope, the primary beam should be adjusted; so as to be parallel to the X-direction of the microscope.

4) Determination the coordinates of each of (A) the center of the interaction, (B) a point in the secondary particle track i.e. $\overrightarrow{AB}$ and $\overrightarrow{AO}$.

$$\overrightarrow{AB} = x_1 \hat{i} + y_1 \hat{j} + z_1 \hat{k} \qquad \text{(II-8)}$$

$$\overrightarrow{AO} = x \hat{i} + y \hat{j} + z \hat{k} \qquad \text{(II-9)}$$

5) So, the space angle (θ) of the secondary particle track is determined by using the equation (II-10)

$$\cos\theta = \frac{\overrightarrow{AB}.\overrightarrow{AO}}{\left|\overrightarrow{AB}\right| \times \left|\overrightarrow{AO}\right|} = \frac{xx_1 + yy_1 + zz_1}{\left(\sqrt{\left(x^2 + y^2 + z^2\right)}\right)\left(\sqrt{\left(x_1^2 + y_1^2 + z_1^2\right)}\right)} \qquad \text{(II-10)}$$

(II-9.4) <u>The Dip Angle Measurement</u>:

Measuring the dip angle (α) of the secondary particle track is performed through the following steps:

1) The nuclear emulsion plate should be placed and fixed on the metal stage of the microscope.

2) The center of the interaction (A) should be adjusted; so as to be coincided with the center of the field of view then focused.

3) Using the rotatable metal stage of the microscope, the primary beam should be adjusted; so as to be parallel to the X-direction of the microscope then moving in the backward direction the rotatable metal stage of the microscope a distance 3000μm along the primary beam.

4) Using the rotatable metal stage of the microscope, the secondary particle track; should be adjusted; so as to be parallel to the X-direction of the microscope then moving in the forward direction the rotatable metal stage of the microscope a distance 2000μm along the secondary particle track.

5) Determination the (Z) coordinate with respect to the glass of each of (A) the center of the interaction i.e.(Z_{star}), (B) a point in the secondary particle track" i.e.(Z_{Track}) and at the distance 3000μm i.e.(Z_{Beam}).

6) Notice that the shrinkage factor(K) is given by the equation.

7) By taken in our consideration that the primary beam has small deviation $(\alpha_\circ)$ from the nuclear emulsion plane (XOY) plane given by the equation (II-11).

$$\alpha_\circ = \tan^{-1}\left(K\left(Z_{star} - Z_{Beam}\right) \Big/ X_{Beam} \right) \qquad \text{(II-11)}$$

8) The dip angle (α) of the secondary particle track is given by the equation (II-12)

$$\alpha = \tan^{-1}\left(K\left(Z_{Track} - Z_{star}\right) \Big/ X_{Track} \right) \qquad \text{(II-12)}$$

9) The true dip angle $\left(\alpha^{'}\right)$ of the secondary particle track is given by the equation (II-13)

$$\alpha^{'} = \left(\alpha \pm \alpha_{\circ}\right) \qquad \text{(II-13)}$$

CHAPTER III

EXPERIMENTAL RESULTS & DISCUSSIONS

Chapter III

Experimental Results and Discussions

(III-1) Statistical Topology of Experiment:

(III-1.1) Statistical Events Details:

In the present experiment, a stack of FUJI type of nuclear emulsion was exposed to the 14.6A GeV ^{28}Si beam at Brookhaven National Laboratory (BNL) Alternating Gradient in Synchrotron (AGS). The dimensions of each emulsion pellicle are 20 cm ×10 cm ×600 μm thickness (before development), with sensitivity of about 30 grains per 100 μm for the minimum ionizing particles. The chemical composition of FUJI emulsion is given in section (II-2).The interactions were found by along the track double scanning method, fast in the forward direction and slow in the backward one up to $\approx$7 cm potential path length from the beam entrance. The one prong events with an emission angle of the secondary track ($\theta_{lab} \leq 3^{o}$) and having no visible track from the excitation or disintegration of either the incident projectile or the target nucleus were excluded, as due to elastic scattering of the projectile nuclei. Through a total scanned length of 53.27 m of the primary ^{28}Si beam tracks, 552 inelastic interaction events were detected. The events due to electromagnetic dissociation [31] i.e. with ($N_h = 0$, $n_s = 0$) are excluded into the total number of events.

(III-1.2) The Interaction Mean Free Path:

The experimental value of the average mean free path (λ_{exp}) due to ^{28}Si interactions in the emulsion is found to be 9.65 ± 0.42 cm.The empirical predictions of the average mean free paths could be obtained from the basis of the Bradt-Peters equation for the interaction cross section [83] discussed in section (I-6). Table (III-1) shows the experimental values of the average mean free paths for the present ^{28}Si beam at 14.6A Gev, together with the data for

the other projectiles(^{1}p,^{2}H,^{3}He,^{4}He,^{6}Li,^{7}Li,^{12}C,^{16}O,^{22}Ne,^{24}Mg,^{28}Si,and^{32}S)[28,84-94] Interacting in nuclear emulsion at incident energy values of (2.2-14.6A GeV) . The value of λ_{exp} for each projectile presented in Table (III-1) is compared with the corresponding empirical values (λ_{cal}) according to equations (I-5) and (I-6). These will be referred to in Table (III-1) as (λ^{a}_{cal}) and (λ^{b}_{cal}), respectively. According to the results of Table (III-1), it may be stated that,

1) The experimental values of average mean free path increase with decreasing the projectile mass number up to (^{22}Ne) where it will take a constant value.
2) In the case of ^{7}Li, λ_{exp} is slightly larger than that of ^{6}Li. This may be due to the special structure of ^{6}Li.
3) The empirical predictions of the mean free path values using the two mentioned formula are considerably in agreement with the corresponding experimental ones. This means that, the interaction cross-section of the nuclei is successfully explained by the geometrical cross section with the overlapping parameter Bradt-Peters equation.

Table (III-1): *The experimental values of average mean free path (λ_{exp}) in the interactions of different projectiles with emulsion nuclei and the corresponding calculated values according to the equations (I-5) and (I-6)((λ^{a}_{cal}) and (λ^{b}_{cal}) respectively).* [28, 84-94]

Projectile	Incident Energy (GeV/A)	λ_{exp} (cm)	λ^{a}_{cal} (cm)	λ^{b}_{cal} (cm)	Ref
p	3.7	30.20±0.70	27.82	35.15	28
^{2}H	3.7	26.90±0.60	23.60	23.74	84,85
^{3}He	3.7	19.74±0.48	21.21	21.22	86
^{4}He	3.7	19.50±0.30	19.43	19.47	87
^{6}Li	3.7	14.54±0.45	17.08	17.13	88,89
^{7}Li	2.2	15.30±0.48	16.21	16.28	88,89
^{12}C	3.7	13.70±0.10	13.36	13.49	84,85
^{16}O	3.7	13.00±0.50	11.95	12.12	90
^{22}Ne	3.2	9.92±0.30	10.49	10.71	91
^{24}Mg	3.7	9.60±0.20	10.12	10.35	92
^{28}Si	3.7	9.12±0.19	9.47	9.72	93
^{28}Si	14.6	9.65±0.42	9.96	10.05	Present work
^{32}S	3.7	9.55±0.34	8.94	9.20	94

(III-1.3) Inelastic Interactions of Silicon Projectile with light (CNO) and heavy (AgBr) Emulsion nuclei:

Figure (III-1) shows the normalized multiplicity distributions of the heavily ionizing particles (N_h) produced in the interactions of ^{28}Si-Em at 14.6A GeV in compared with the corresponding data for interactions of ^{28}Si-Em at 3.7A GeV[93]. We observe that, the two distributions are very similar within experimental errors and independent on the incident energy. These results give evidence for limiting fragmentation hypothesis, which implies that both projectile and target may be fragmented irrespective of each other.

Since the nuclear emulsion is a composite target (see section (II – 2)), therefore the incident silicon will interact with either one of the following groups of target nuclei, the free hydrogen (H), the light group(CNO) and heavy group(Ag Br).

An important parameter which is easy to obtain experimentally and greatly helps of separation of the interactions with the different groups of nuclei(H,CNO,AgBr) is the number of heavily ionizing particles (N_h) ,emitted from each interaction. So a large number of criteria have been proposed to separate the interactions of any projectile due to each group. One of these methods is the integral distribution method [24, 25]. According to this method, the separation of the interactions of any projectile with different group of the emulsion nuclei is as following:

Fig. (III-2) presents the integral distribution of for all events due to the interaction of ^{28}Si with emulsion nuclei at 14.6A GeV as a function of the number of heavily ionizing particles, N_h.

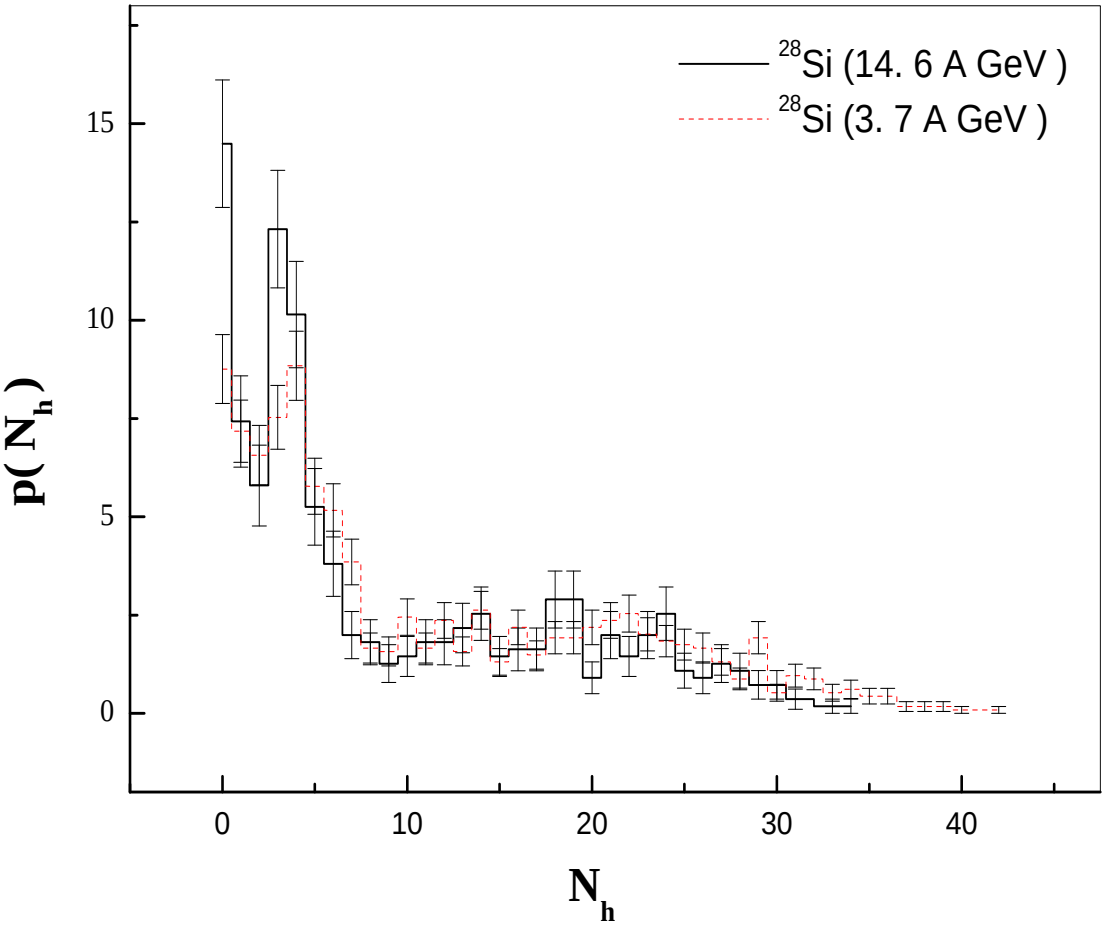

Fig. (III-1): *The normalized multiplicity distributions of the heavily ionizing particles (N_h) produced in the interactions* of *^{28}Si-Em at 14.6A GeV in compared with the corresponding data for interactions of ^{28}Si-Em at 3.7A GeV.*

The separation of the statistical events into groups, according to the target nuclei (H, CNO, and AgBr), can be made by three methods. The first method (Dubna) is executed using Eq. (I-6). While the second method (EMU01) by Eq. (I-5). The third method is called integral distribution method [24, 25]. This method depends mainly on the integral distribution of heavily ionizing particle multiplicity (N_h). The behavior of N_h integral distributions is independent on the mass of the projectile, while it was found to be depending on the target mass.

Fig. (III-2) presents the integral distribution of N_h through the interaction of ^{28}Si at 14.6A GeV with emulsion nuclei.

According to integral distribution method, one can classify the sample of events as,

- The group of events at (N_h = 0, 1) mainly represents the interactions with a free hydrogen (H), in addition to those with (CNO) and (AgBr).
- The group of events having (N_h = 2-8) may correspond to the interaction with light nuclei (CNO) in addition to peripheral collisions with heavy nuclei (AgBr).
- The group of events at (N_h > 8) represents the interactions with AgBr nuclei.

In Fig. (III-2), it was found that four distinct straight line segments can fit the data well. The intersection point of the 1st and 2nd lines is positioned at N_h =8. From the fitting parameters of the 1st line, its intersection point with y-axis $\approx$ 496.since the total sample of events due to H targets are (552-496) = 56 events. The fitting parameters of the 2nd line give its intercept as = 302. Therefore, the sample of events due to CNO is (496-302) = 194 events. The events due to the interactions with AgBr are = 302.

In this work, the percentage of events due to the interactions of ^{28}Si with different emulsion groups according to the three mentioned methods of target separation were calculated and presented in Table (III-2).

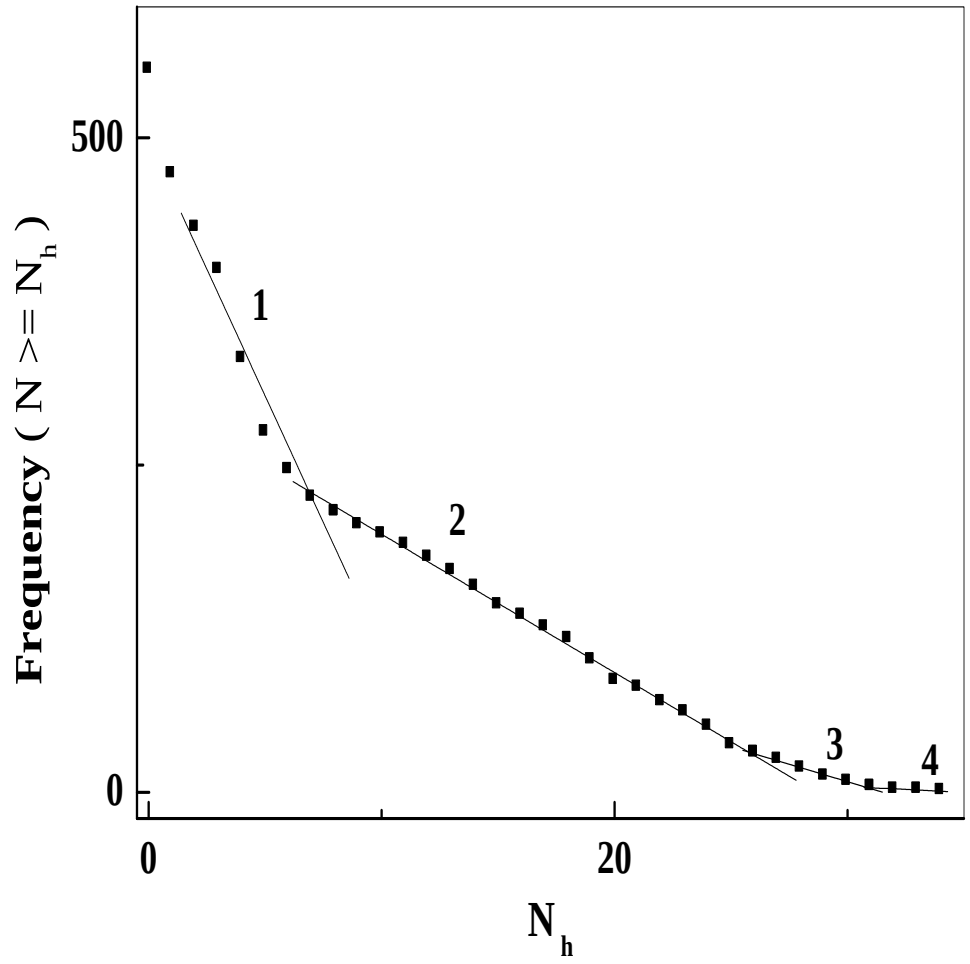

Fig. (III-2): *The integral frequency distribution as a function of* N_h *for* $^{28}Si - Em$ *interactions at 14.6A GeV.*

Table (III-2): *The percentage of events due to the interaction of ^{28}Si at 14.6A GeV with different emulsion groups of nuclei and their percentages using three methods of separation.*

Separation method	H	CNO	AgBr
Integral distribution method	10±1%	35±2%	55±2%
Dubna equation	14±1%	32±2%	54±2%
EMU01 equation	13±1%	33±2%	54±2%

(III-2) Multiplicity Characteristics:

The multiplicity characteristics of different emitted secondaries from the interactions of any projectile provide a valuable tool to investigate the mechanism of the particle production in nucleus-nucleus interactions. In the present work, the focusing will be on the production of the fast and slow target protons in the forward (FHS) and backward (BHS) hemispheres of the interaction.

(III-2.1) Average Multiplicities:

Now, Table (III-3) displays the average multiplicity of shower, grey, black, and heavily ionizing particles produced in ^{28}Si interactions with emulsion nuclei at 3.7-14.6A GeV. The average multiplicities of the particles emitted in FHS and BHS are also shown in Table (III-3).

Table (III-3): *The values of average multiplicities of the different emitted secondaries in interaction of ^{28}Si at 14.6A GeV with emulsion nuclei in comparison with the corresponding data for ^{28}Si-Em at 3.7A GeV [93].*

Total sample	^{28}Si (3.7A GeV)	^{28}Si (14.6A GeV)
$\langle n_s \rangle$	15.01±0.34	28.92±1.21
$\langle n_s^f \rangle$	14.62±0.33	28.42±1.18
$\langle n_s^b \rangle$	0.39±0.02	0.49±0.04
$\langle N_g \rangle$	3.71±0.12	3.01±0.16
$\langle N_g^f \rangle$	2.99±0.10	2.26±0.13
$\langle N_g^b \rangle$	0.72±0.03	0.74±0.05
$\langle N_b \rangle$	7.14±0.20	5.67±0.24
$\langle N_b^f \rangle$	4.39±0.13	3.17±0.14
$\langle N_b^b \rangle$	2.76±0.08	2.51±0.12
$\langle N_h \rangle$	10.85±0.29	8.68±0.37

(III-3) Grey Particles Multiplicity Characteristics:

(III-3.1) Multiplicity Distributions of Grey Particles:

Figure (III-3) shows the normalized experimental multiplicity distributions of grey particles for the interactions of ^{28}Si with emulsion nuclei at 14.6A GeV compared with the corresponding data for ^{28}Si-Em at 3.7A GeV[93].

From fig. (III-3), one can observe that, the two distributions are nearly similar within experimental errors and independent on the incident energy.

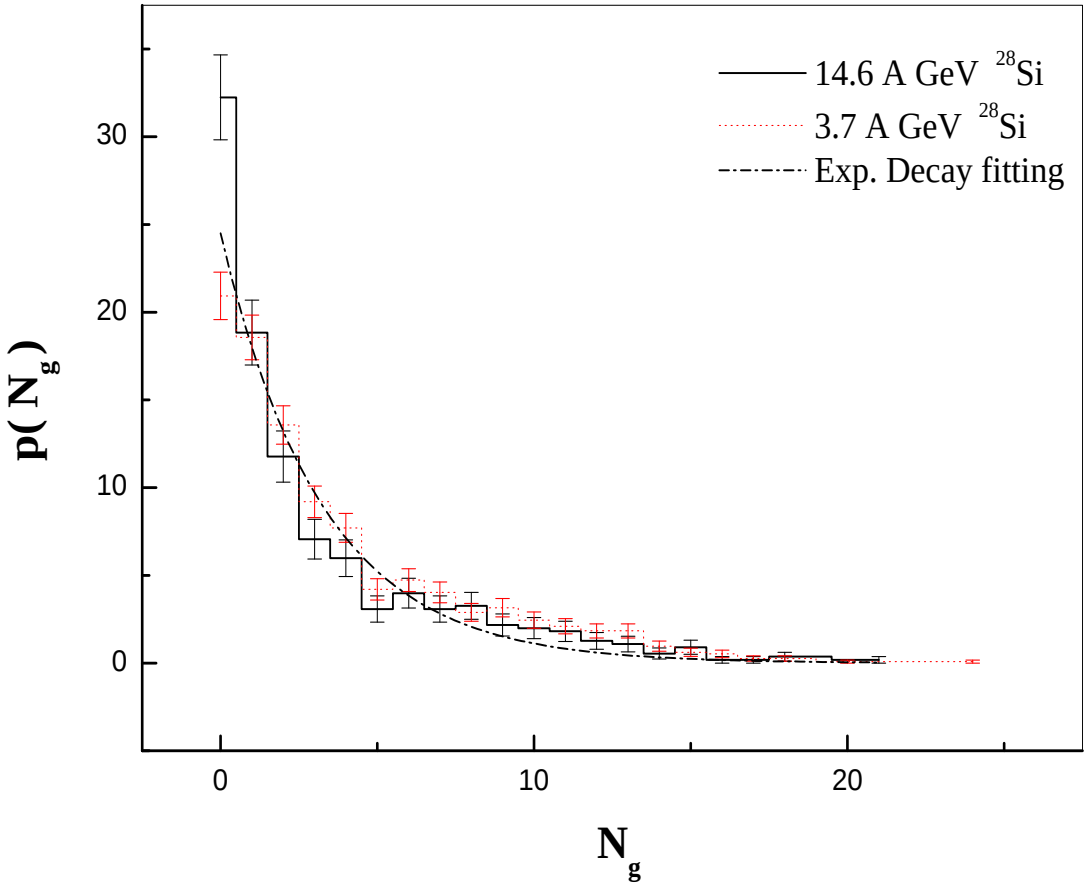

Fig. (III-3): *The normalized multiplicity distributions for the grey particles through the interactions of ^{28}Si with emulsion nuclei at 14.6A GeV in comparison with the corresponding data for ^{28}Si-Em at 3.7A GeV.*

(III-3.2) The Probability of the Interactions Accompanied by Backward Emission of Grey Particles:

Table (III-4) presents the probabilities of observing events accompanied by backward grey particles ($N_g^b>0$) in the interactions of ^{28}Si at 14.6A GeV with emulsion nuclei. Our experimental data are compared with analogical data in interactions of ^{4}He, ^{6}Li, ^{7}Li and ^{28}Si at 3.7A GeV with emulsion nuclei.

From the data in table (III-4),

1- It is interesting to notice that the percentage number of events accompanied by backward g-particles emission tend to be constant.

2- One can conclude that it is independent on the projectile size and energy.

Table (III-4): *The percentage number of events accompanied by backward g-particles in the interactions of 14.6 A GeV ^{28}Si-Em and the data of the other projectiles.* [93, 95, 96]

Projectile	Energy A GeV	Total sample	Percentage	Ref.
^{4}He	3.7	1092	34.25±1.77	95
^{6}Li	3.7	1021	46.32±2.13	96
^{7}Li	2.2	1011	35.19±1.87	96
^{28}Si	3.7	1142	39.23±1.85	93
^{28}Si	14.6	552	36.23±3.39	Present work

(III-3.3) Multiplicity Distributions of Forward-backward Grey Particles:

Fig. (III-4) shows the normalized multiplicity distributions for the grey particles $[P(n_g^f)]$ and $[P(n_g^b)]$, emitted in FHS and BHS respectively for the interactions of ^{28}Si with emulsion nuclei at 14.6A GeV. For sake of comparison, the obtained results are displayed together with the corresponding data for ^{28}Si –Em interactions at 3.7A GeV[93].

From Fig. (III-4a), one can observe that, the two distributions are nearly similar within experimental errors, i.e. independent on the incident energy.

On the other hand, fig. (III-4b) shows that the distributions of the grey particles emitted in BHS are found to be nearly the same for the two incident energies. Therefore one can say that, there is no dependence of backward grey particles production on incident energy. This confirms the existence of limiting fragmentation hypothesis in the backward production of fast target protons. All the normalized distributions in FHS and BHS are fitted well by exponential decay law of the form,

$$P(N_g^i) = \alpha_g^i e^{-\lambda_g^i N_g^i} \qquad \text{(III-1)}$$

Where α_g^i and λ_g^i are the fitting parameters.

[g(grey)] and [i=f(forward),b(backward)]

The above relation (III-1) represents the fundamental equation of the decay of an excited system, which emits the grey particles in FHS and BHS. The values of decay constant λ_g^i and α_g^i for different projectiles which obtained from the best fitting of experimental data with the above decay equation are listed in table (III-6).

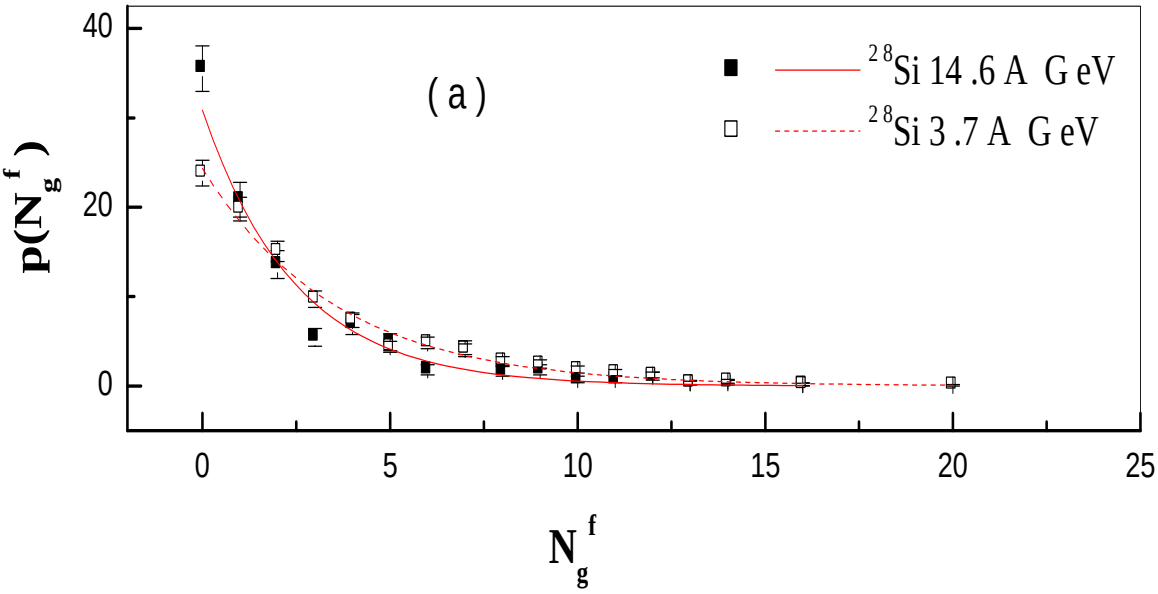

Fig. (III-4a): *The normalized multiplicity distributions of the grey particles emitted in FHS through the interactions of Si^{28} at (3.7and14.6A GeV) with emulsion nuclei together with the smooth fitting curve.*

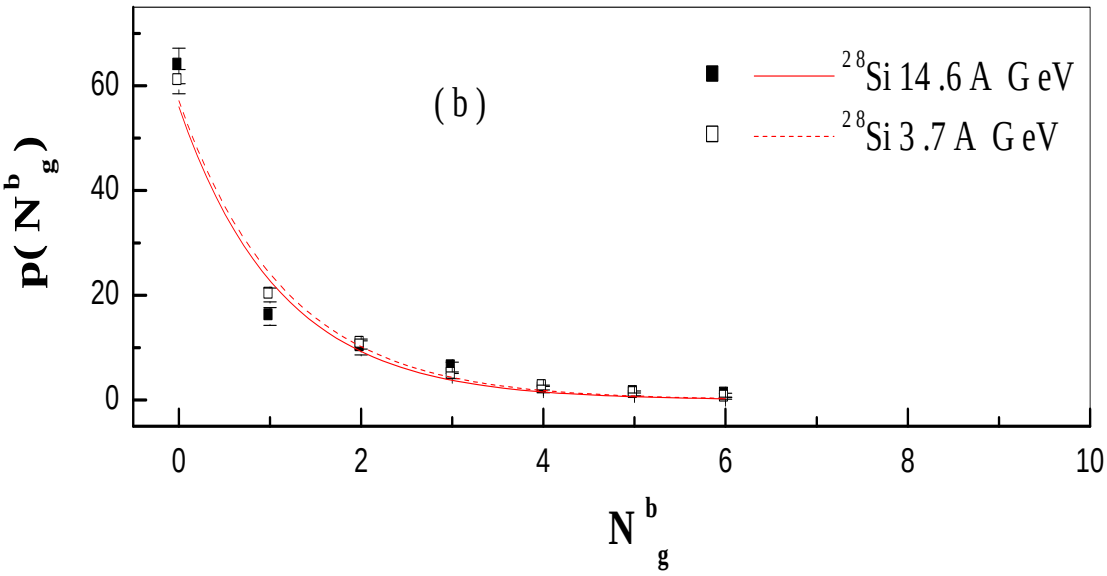

Fig.(III-4b): *The normalized multiplicity distributions of the grey particles emitted in BHS through the interactions of Si^{28} at (3.7and14.6A GeV) with emulsion nuclei together with the smooth fitting curve.*

(III-3.4) Average Multiplicity of Grey Particles:

Table (III-5) presents the average values of the grey particle multiplicity, $\langle N_g^f \rangle$ and $\langle N_g^b \rangle$, emitted in FHS and BHS, respectively for the interactions of the present 14.6A GeV ^{28}Si in nuclear emulsion. These data are compared with the corresponding data due to the interactions of different projectiles with emulsion nuclei (P, ^{3}He, ^{4}He, ^{6}Li, ^{7}Li, ^{28}Si and ^{32}S) [87, 93, 97, 98, and 99] at (2.2-14.6A GeV).

The forward to backward ratios $(F/B)_g$ which are defined as the ratios between the average multiplicities of the forward emitted grey particles to those of backward ones, are displayed in Table (III-5). The $(F/B)_g$ represents the anisotropy ratio of angular distribution which determined according to statistical model in section (I-8) by the following equations,

$$(F/B)_g \approx \exp\left[\frac{4}{\sqrt{\pi}}\chi_o^{\,g}\right] \qquad \text{(III-2)}$$

Where $\chi_o^{\,g}$ is the predicted rational velocity.

$$\chi^g{}_o = \beta_{//}^{\,g} / \beta_o^{\,g} \qquad \text{(III-3)}$$

Where $\beta_{//}^{\,g}$ the mean longitudinal velocity of the center mass of the grey particle emission system and $\beta_o^{\,g}$ is the characteristic spectral velocity of the fragmentation system of grey particles.

From ref (92) the value of $\beta_o^{\,g} \approx 0.35$

The values of $\beta_{//}^{\,g}$ can be calculated from the equation,

$$\beta_{//}^{\,g} = \beta_o^{\,g}\chi_o^{\,g} \qquad \text{(III-4)}$$

Table (III-5): *The average multiplicity of the grey particles emitted in FHS and BHS from different projectiles interactions with emulsion nuclei at high energy*.

Projectile	Energy (**GeV**/A)	$\langle N_g^f \rangle$	$\langle N_g^b \rangle$	$(F/B)_g$	χ_o^g	$\beta_{//}^g$	Ref
p	3.7	1.31±0.03	0.45±0.01	2.92±0.11	0.47	0.16	93
^{3}He	3.7	1.92±0.06	0.61±0.03	3.12±0.16	0.51	0.17	87
^{4}He	2.1	1.97±0.05	0.63±0.02	3.15±0.14	0.51	0.17	93
^{4}He	3.7	1.91±0.07	0.67±0.04	2.86±0.19	0.46	0.16	87
^{6}Li	3.7	2.08±0.08	0.95±0.05	2.18±0.13	0.35	0.12	97
^{7}Li	2.2	1.78±0.07	0.64±0.04	2.80±0.19	0.45	0.16	97
^{28}Si	3.7	2.99±0.10	0.72±0.03	4.12±0.23	0.63	0.22	93
^{28}Si	14.6	2.26±0.13	0.74±0.05	3.05±0.27	0.49	0.17	Present work
^{32}S	3.7	3.19±0.14	0.82±0.05	3.19±0.29	0.52	0.18	98, 99

From Table (III-5) one can notice that,

- For light projectile (P, ^{3}He, ^{4}He, ^{6}Li, ^{7}Li) [87, 93, 97], the values of $\langle N_g^f \rangle$ tend to be constant within the experimental errors. Their values are ≈ 2.
- For heavier projectiles i.e. (^{28}Si and ^{32}S) [93, 98, 99] the values of $\langle N_g^f \rangle$ tend to be ≈ 3.
- The behavior of $\langle N_g^b \rangle$ values is the same like that of $\langle N_g^f \rangle$ but with lower values. The values of $\langle N_g^f \rangle$ are nearly three times greater than $\langle N_g^b \rangle$ for all projectiles.
- The result is reflected on the $(F/B)_g$ and consequently on the values of χ_o^{g} which tend to be nearly constant within experimental errors overall projectiles. Therefore, mainly one concludes that, the dependence of the fast target fragments (g-particles) in FHS and BHS on the projectile sizes is nearly weak.
- The values of $\chi_o^{g} \approx 0.5$ for different projectile studied here.
- The emitting system of the g- particles is fast and with typical longitudinal velocities $\beta_{//}^{g} \approx 0.13\text{-}0.22$

(III-4)Target Dependence

(III-4.1)Multiplicity Distributions of Grey Particles:

Fig. (III-5) shows the multiplicity distributions of grey particles emitted in FHS and BHS through the interactions of ^{28}Si with nuclear emulsion at 14.6A GeV. In order to study the dependence of the multiplicity distribution on the target size, our sample is classified according to the target size into three groups (H, CNO, and AgBr). In Fig. (III-5), one can observe the effect of the target size on the multiplicity of the forward and backward emitted grey particles. In FHS and BHS the grey particles multiplicity distributions show exponential decay shapes. These shapes are well fitted by the formula

$$P\left(N_g^i\right) = \alpha_g^i e^{-\lambda_g^i N_g^i} \qquad \text{(III-5)}$$

Where α_g^i and λ_g^i are the fitting parameters.

[g(grey)] and [i=f(forward),b(backward)]

The above relation (III-5) represents the fundamental equation of the decay of an excited system, which emits the grey particles in FHS and BHS. The values of decay constant λ_g^i and α_g^i for different projectiles which obtained from the best fitting of experimental data with the above decay equation are listed in table (III -6).

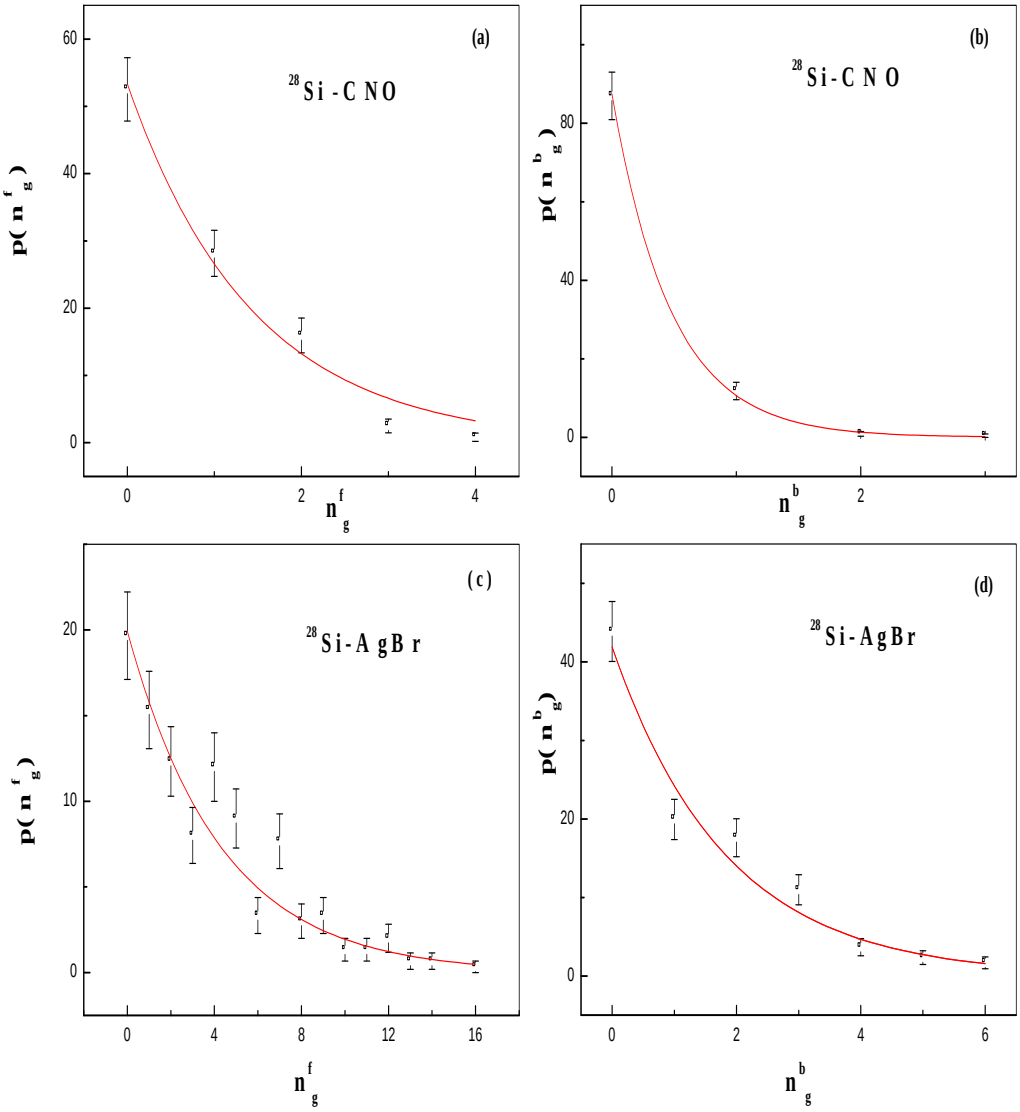

Fig. (III-5): *The multiplicity distribution emitted grey particles in the interactions of the present 14.6A GeV ^{28}Si with different target groups of emulsion nuclei (CNO) in the forward (a) ,the backward (b) and (AgBr) in the forward (c)and the backward (d) together with the exponential decay curves.*

Table (III-6): *The fitting parameters of forward and backward emitted grey particle distributions fitted by an exponential decay law form* [93, 95, 100,101]

Projectile	Incident energy A GeV	Target	α_g^f	λ_g^f	α_g^b	λ_g^b	Ref.
^{4}He	3.7	Em	33.94±1.40	0.43±0.02	59.76±2.26	0.97±0.04	95
^{12}C	3.7	Em	……	…….	45.92±11.56	0.75±0.06	100
^{22}Ne	3.3	Em	……	…….	40.91±7.58	0.66±0.04	100
^{28}Si	14.6	CNO	53.32±3.23	0.69±0.17	87.41±6.02	2.11±0.04	Present work
		Em	30.85±1.88	0.41±0.13	55.97±3.08	0.89±0.04	
		AgBr	19.92±1.65	0.23±0.31	41.89±3.17	0.55±0.13	
^{28}Si	3.7	CNO	……	……..	85.15±0.48	1.88±0.04	93
		Em	24.58±0.62	0.28±0.01	57.13±2.08	0.86±0.03	
		AgBr	……..	……..	46.54±2.19	0.63±0.03	
^{16}O	3.7	CNO	……...	…….	77.53±2.72	1.52±0.05	101
		Em	……...	…….	44.76±1.33	0.60±0.02	
		AgBr	……...	…….	27.04±1.12	0.38±0.01	

From table (III-6) it is clearly seen that, the values of the decay constant λ_g^b are nearly constant within experimental error and independent on the projectile incident energy. On the other hand, one can observe that the values of λ_g^f and λ_g^b decreases with increasing the target size.

Consequently the probability of grey particle production in BHS will increase with target size.

(III-4.2) Average multiplicity of grey particles:

The average multiplicity of forward and backward emitted grey particles in the interactions of the present 14.6A GeV ^{28}Si with different groups of emulsion nuclei, are tabulated in Table (III-7),

From Table (III-7) it is noticed that,

- The strong dependence of the grey particles multiplicity in both FHS and BHS on the target size.
- The values of $(F/B)_g$ begin to be constant within experimental error.

Table (III-7): *The average multiplicity of forward and backward emitted grey particles in the interactions of 14.6A GeV ^{28}Si with different groups of emulsion nuclei.*

Target	$\langle N_g^f \rangle$	$\langle N_g^b \rangle$	$(F/B)_g$
CNO	0.84±0.06	0.18±0.03	4.65±0.95
Em	2.26±0.13	0.74±0.05	3.05±0.27
AgBr	3.66±0.19	1.26±0.08	2.89±0.25

(III-5) The Black Particle Multiplicity Characteristics:

(III-5.1) Multiplicity Distributions of Black Particles:

Figure (III-6) presents the normalized experimental multiplicity distributions of black particles for the interactions of ^{28}Si at 14.6A GeV with emulsion nuclei compared with the corresponding data of ^{28}Si at 3.7A GeV[93]. From fig. (III-6), one can observe that, the two distributions are nearly similar within experimental errors and independent on the incident energy.

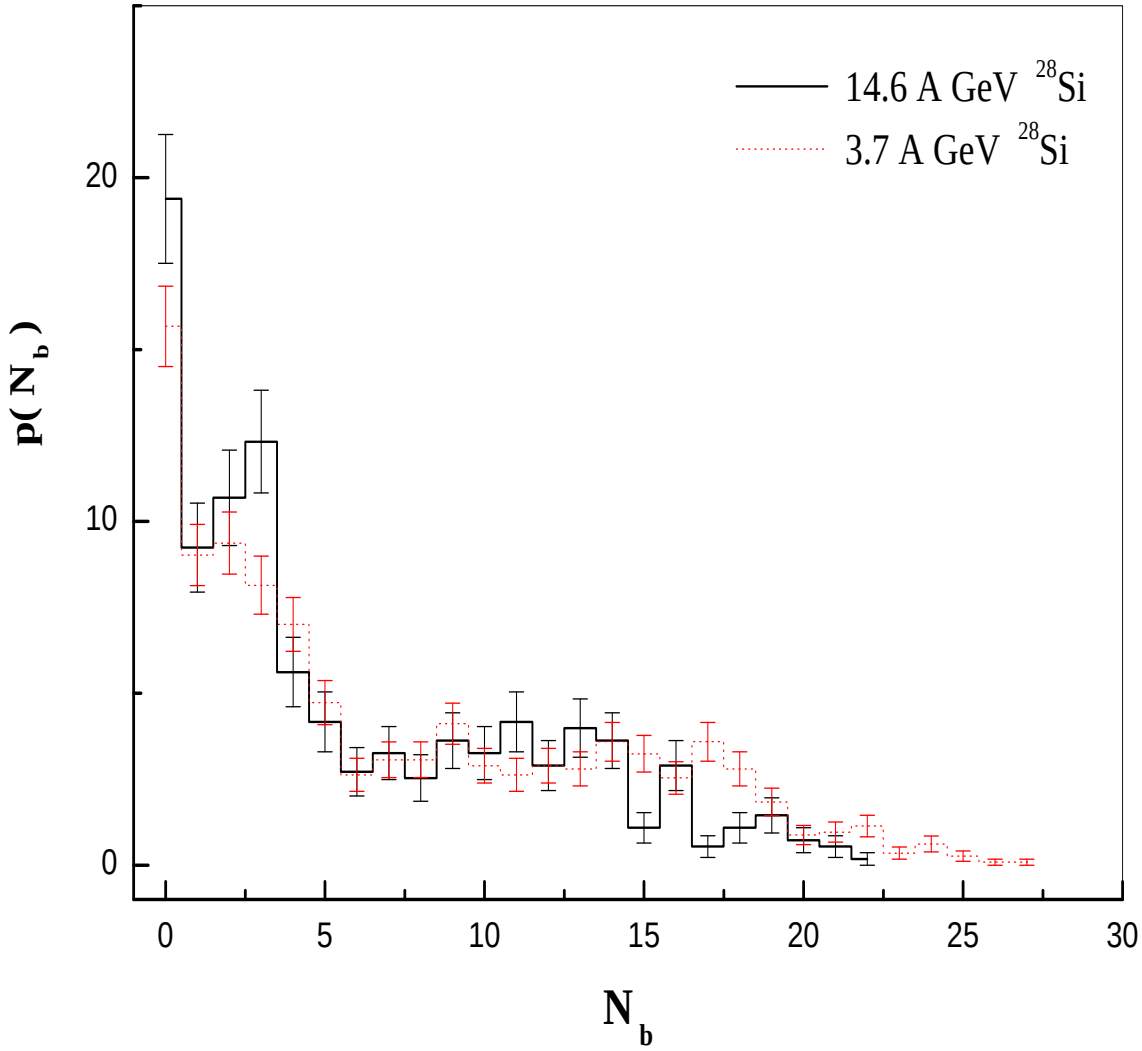

Fig. (III-6): *The normalized multiplicity distributions of the black particles through the interactions of ^{28}Si at (3.7and 14.6A GeV) with emulsion nuclei.*

(III-5.2) The Probability of the Interactions Accompanied by Backward Emission of Black Particles:

Table (III-8) presents the probabilities of observing events accompanied by backward black particles ($N_b^b>0$) in the interactions of ^{28}Si at 14.6A GeV with emulsion nuclei. Our experimental data are compared with analogical data in interactions of ^{4}He, ^{6}Li, ^{7}Li and ^{28}Si at 3.7A GeV with emulsion nuclei.

From the above data in table (III-8),

1- It is interesting to notice that the percentage number of events accompanied by backward b-particles emission tend to be constant.

2- One can conclude that it is independent on the projectile size and incident energy.

Table (III-8): *The percentage number of events accompanied by backward b-particles in the interactions of ^{28}Si-Em at 14.6 A GeV and the corresponding data of the other projectiles.* [93, 95, 96]

Projectile	Energy A GeV	Total sample	Percentage	Ref.
^{4}He	3.7	1092	64.56±2.43	95
^{6}Li	3.7	1021	67.81±2.58	96
^{7}Li	2.2	1011	69.59±2.63	96
^{28}Si	3.7	1142	70.23±2.48	93
^{28}Si	14.6	552	67.75±2.42	Present work

(III-5.3) Multiplicity Distributions of Forward-Backward Black Particles:

Fig. (III-7) shows the normalized multiplicity distributions of the slow target protons (black particles) in the forward p(N^f_b) and backward p(N^b_b)hemispheres produced from the interactions of ^{28}Si at 14.6A GeV with emulsion nuclei. For comparison the same data for ^{28}Si –Em at 3.7A GeV [93]are presented in Fig. (III-7).

From Fig. (III-7a) one can observe that, the black particles emitted in FHS have nearly similar multiplicity distributions for the two energies (3.7-14.6A GeV) and longer in ^{28}Si at 3.7A GeV.

Also from fig. (III-7b) one can observe that, the black particles emitted in BHS have very similar multiplicity distributions for the two energies (3.7-14.6 A GeV).Therefore one can say that, there is no dependence of backward black multiplicity distributions in both hemispheres on projectile energy.

It is interesting to notice that, all distributions can be fitted by exponential decay curves given by the formula,

$$P\left(N_b^i\right) = \alpha_b^i e^{-\lambda_b^i N_b^i} \qquad \text{(III-6)}$$

Where α_b^i and λ_b^i are the fitting parameters.

[b (black)] and [i=f(forward),b(backward)]

The above relation (III-6) represents the fundamental equation of the decay of an excited system, which emits the black particles in FHS and BHS. The values of decay constant λ_b^i and α_b^i for different projectiles which obtained from the best fitting of experimental data with the above decay equation are listed in table (III-9).

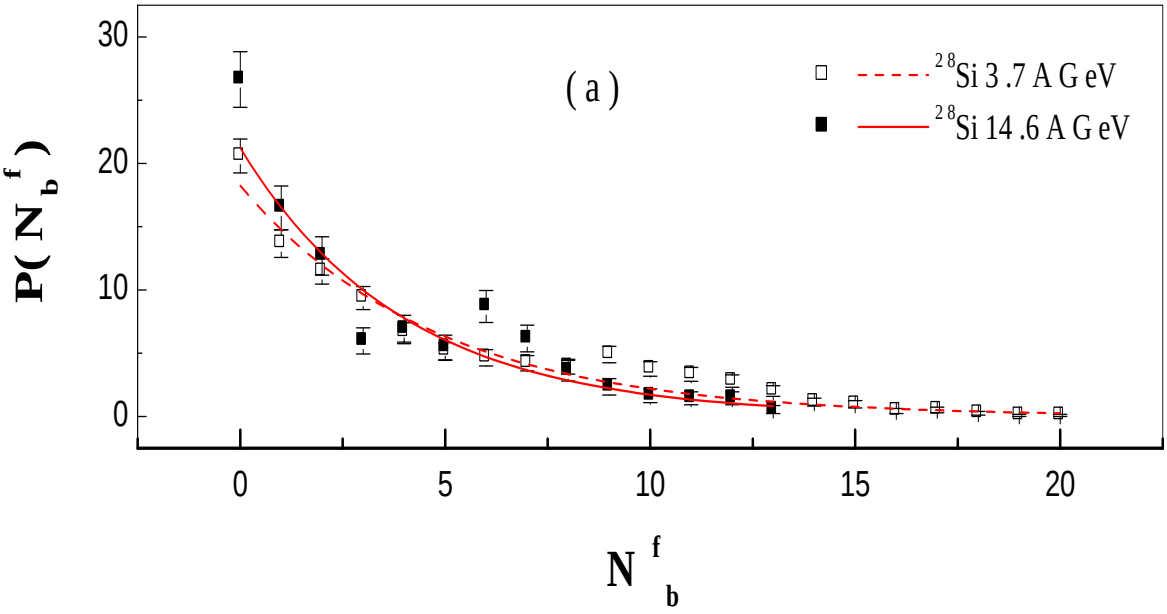

Fig. (III-7a): *The normalized multiplicity distributions of the black particles emitted in FHS through the interactions of Si^{28} at (3.7and14.6A GeV) with emulsion nuclei, together with the smooth curve fitting.*

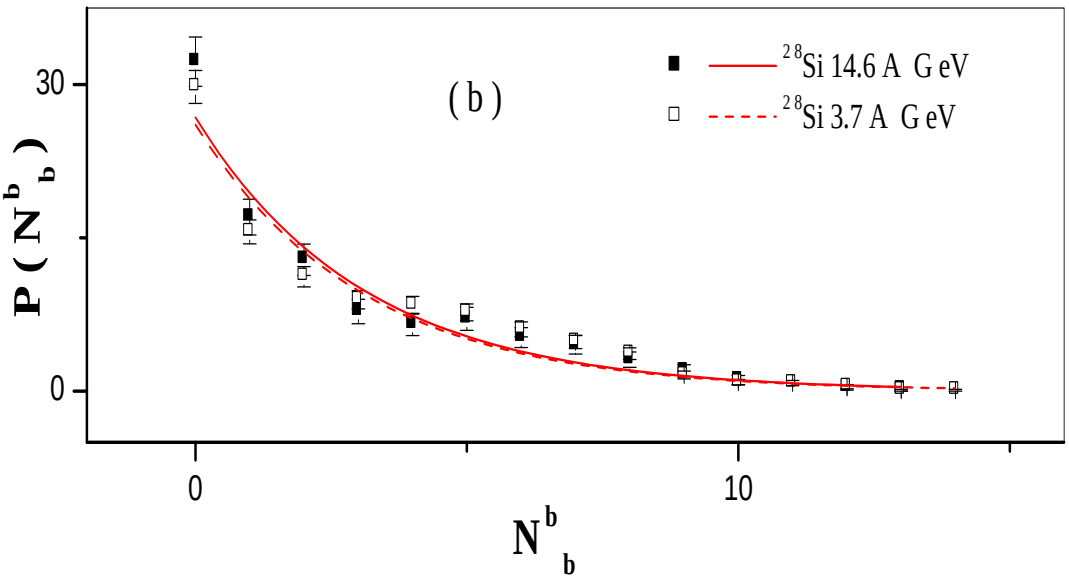

Fig. (III-7b): *The normalized multiplicity distributions of the black particles emitted in BHS through the interactions of Si^{28} (3.7and14.6A GeV) with emulsion nuclei, together with the smooth curve fitting.*

Table (III-9): *The characteristic parameters of multiplicity distributions of black particles emitted in FHS and BHs through nucleus-nucleus interactions at high energy.* [87, 93, 97, 98, 99]

Projectile	Energy (GeV/A)	Target	α_b^f	λ_b^f	α_b^b	λ_b^b	Ref
^{3}He	3.7	Em	21.90±0.74	0.25±0.01	28.17±0.94	0.34±0.01	87
^{4}He	2.1	Em	22.25±0.67	0.26±0.01	29.23±0.86	0.35±0.01	93
^{4}He	3.7	Em	25.63±1.08	0.31±0.01	30.78±1.26	0.38±0.01	87
^{6}Li	3.7	Em	25.69±1.09	0.30±0.01	31.82±1.31	0.40±0.01	97
^{7}Li	2.2	Em	22.38±0.98	0.26±0.01	29.80±1.27	0.36±0.01	97
^{28}Si	3.7	Em	18.24±4.72	0.21±0.01	26.07±1.04	0.33±0.01	93
^{28}Si	14.6	CNO	44.79±3.61	0.63±0.11	51.74±4.11	0.73±0.11	Present work
		Em	21.23±1.35	0.25±0.24	26.78±1.59	0.32±0.16	
		AgBr	……..	……..	…….	…….	
^{32}S	3.7	Em	16.25±0.96	0.20±0.01	25.34±1.37	0.32±0.01	98,99

From Table (III-9) one can notice that,

- The values of fitting parameters $\alpha_b^{f,b}$ and $\lambda_b^{f,b}$ are nearly constant and independent on the projectile size and incident energy.
- The values of the fitting parameters $\alpha_b^{f,b}$ and $\lambda_b^{f,b}$ are dependent on the target size.

Hence, the mechanism responsible for producing black particles in FHS may be similar to that in BHS.

(III-5.4) Average multiplicity of black particles:

Table (III-10) gives the average multiplicity values of the black particles emitted in FHS and in BHS, through the interactions of ^{28}Si with emulsion nuclei at 14.6A GeV. The data are compared with those of (P, ^{3}He, ^{4}He, ^{6}Li, ^{7}Li, and ^{32}S) [87, 93, 97, 98 and 99] at (2.1-14.6A GeV).

The predicted rational velocity χ_o according to statistical model in section (I-8) will be given by the following equations**,**

$$(F/B)^b \approx \exp\left[\frac{4}{\sqrt{\pi}}\chi_o{}^b\right]. \qquad \text{(III-7)}$$

$$\chi_o{}^b = \beta_{//}{}^b / \beta_o{}^b \qquad \text{(III-8)}$$

Which is the ratio of the longitudinal velocity of the center of mass $\beta_{//}{}^b$, to the characteristic spectral velocity, $\beta_o{}^b$ of the fragmentation system of black particles. So the values of the $\beta_{//}{}^b$, longitudinal velocity of the black particle emitting system for the values of $\beta_o{}^b$ which can be deduced by the following equation,

$$\beta_{//}{}^b = \beta_o{}^b \ \chi_o{}^b \qquad \text{(III-9)}$$

From ref (92) take the value of $\beta_o{}^b \approx 0.11$

Table (III-10): *The average multiplicity of the black particles emitted in FHS and BHS from the interactions of different projectiles with emulsion nuclei at high energy.*

Projectile	Energy (GeV/A)	$\langle N_b^f \rangle$	$\langle N_b^b \rangle$	$(F/B)_b$	x_o^b	$\beta_{//}{}^b$	Ref
p	3.7	3.92±0.01	2.94±0.04	1.33±0.03	0.13	0.014	93
^{3}He	3.7	3.46±0.09	2.39±0.06	1.46±0.05	0.17	0.018	87
^{4}He	2.1	3.42±0.08	2.40±0.06	1.43±0.05	0.16	0.017	93
^{4}He	3.7	2.90±0.10	2.18±0.08	1.33±0.07	0.13	0.014	87
^{6}Li	3.7	2.84±0.09	2.18±0.07	1.29±0.06	0.12	0.013	97
^{7}Li	2.2	3.39±0.12	2.29±0.08	1.48±0.07	0.17	0.018	97
^{28}Si	3.7	4.39±0.13	2.76±0.08	1.59±0.07	0.17	0.018	93
^{28}Si	14.6	3.17±0.14	2.51±0.12	1.26±0.08	0.11	0.012	Present work
^{32}S	3.7	4.63±0.18	2.93±0.12	1.58±0.09	0.21	0.023	98,99

From Table (III-10) one can notice the following:

- The values of $\langle N_b^f \rangle$ and $\langle N_b^b \rangle$ are independent on the projectile size and incident energy, where $\langle N_b^f \rangle \approx 3$ while $\langle N_b^b \rangle \approx 2$, for all interaction.
- The anisotropy ratio $(F/B)_b$ fluctuates around ~1.4, independent on the projectile size or incident energy. The observed constancy, in the anisotropy ratios, indicates a limiting behavior for the system emitting black particles at relativistic energy.
- The predicted rational velocity $\chi_o{}^b$ to be ~ 0.13 for the system of black particle emission.
- The emitting system of the b- particles is slow and its typical longitudinal velocity takes the values in the range $\beta_{//}{}^b \approx 0.012\text{-}0.023$

(III-6) Target Dependence

(III-6.1) Multiplicity distributions of black particles

Fig. (III-8) shows the multiplicity distributions of black particles in forward and backward hemispheres emitted from the interactions of ^{28}Si at 14.6A GeV with different emulsion targets (CNO and AgBr).

From fig. (III-8) a,b one can notice that, the multiplicity distributions p($N_b^{f,b}$) for the interactions of ^{28}Si with light target (CNO) can be fitted with one smooth curve which reflects the same effect of C,N,O targets. On the other hand, Fig (III-8) c, d represents the interactions with heavy target AgBr .It is seen that the experimental points can be explained by two fits with two peaks due to large difference between the size of the two targets Br and Ag.

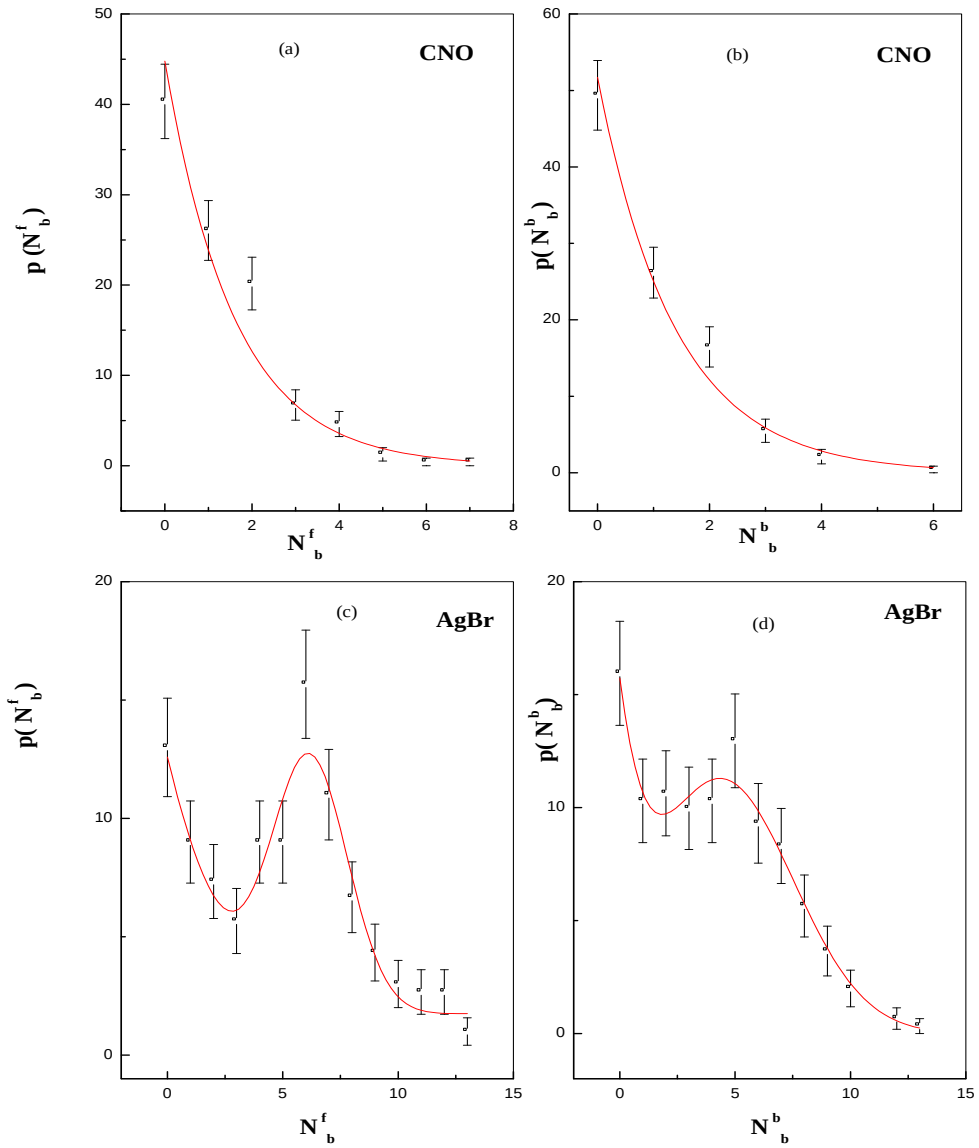

Fig. (III-8): *The normalized multiplicity distribution emitted black particles in the interactions of the present 14.6A GeV ^{28}Si with different target groups of emulsion nuclei (CNO) in the forward (a) ,the backward (b) and (AgBr) in the forward (c)and the backward (d) together with the exponential decay curves.*

(III-6.2) Average multiplicity of black particles:

Table (III-11) gives the average multiplicity of black particles emitted in FHS and BHS through the interactions of ^{28}Si at 14.6A GeV with different groups of emulsion nuclei.

From Table (III-11) one can observe that,

- The dependence on the target size is strong for black particles emitted both in FHS as well as in BHS.
- The constancy in the values of $(F/B)_b$ ~1.3, irrespective of the target size
- The observed constancy, in the anisotropy ratios (F/B), indicates a limiting behavior for the system of black particles emission at relativistic energy.

Table (III-11): *The average multiplicity of forward and backward black particles emitted in the interactions of ^{28}Si at 14.6A GeV with different emulsion groups of nuclei.*

Target	$\langle N_b^f \rangle$	$\langle N_b^b \rangle$	$(F/B)_b$
CNO	1.44±0.11	1.06±0.08	1.35±0.14
Em	3.17±0.14	2.51±0.12	1.26±0.08
AgBr	5.01±0.19	4.00±0.16	1.25±0.07

(III-7)The Multiplicity Correlations:

In nucleus- nucleus interactions, a more sensitive characteristic to understand the mechanism of forward and backward particles productions is the correlations among the multiplicities of the different types of the emitted particles.

Now, the effect of the target size on the multiplicity of the outgoing particles will be studied by the correlations between the mean values of the different emitted particles and different values of (N_h).

Fig.(III-9) through fig. (III-12) give the dependence of the experimental average multiplicities of different types of particles emitted from interaction of ^{28}Si (14.6 A GeV) with emulsion nuclei, on the number of target fragments (N_h). The straight lines in those figures are the results of the linear fitting of the experimental data.

Now, the effect of the target size on the outgoing protons emitted in the first stage of interaction (detected as grey particles) in the forward and backward hemisphere is studied in Fig. (III-9).In this figure the dependence of the experimental average multiplicities of the grey particles emitted in the forward hemisphere $< N^f_g >$ and that emitted in the backward hemisphere $< N^b_g >$ on (N_h) for the interaction of ^{28}Si (14.6 GeV) are displayed.

The Linear fitting of the experimental data is made up to =26.

From the figure, it can be deduced that,

- The values of$< N^f_g >$ and $< N^b_g >$ tend to increase linearly with increasing the target size (N_h-values) in a strong dependence.

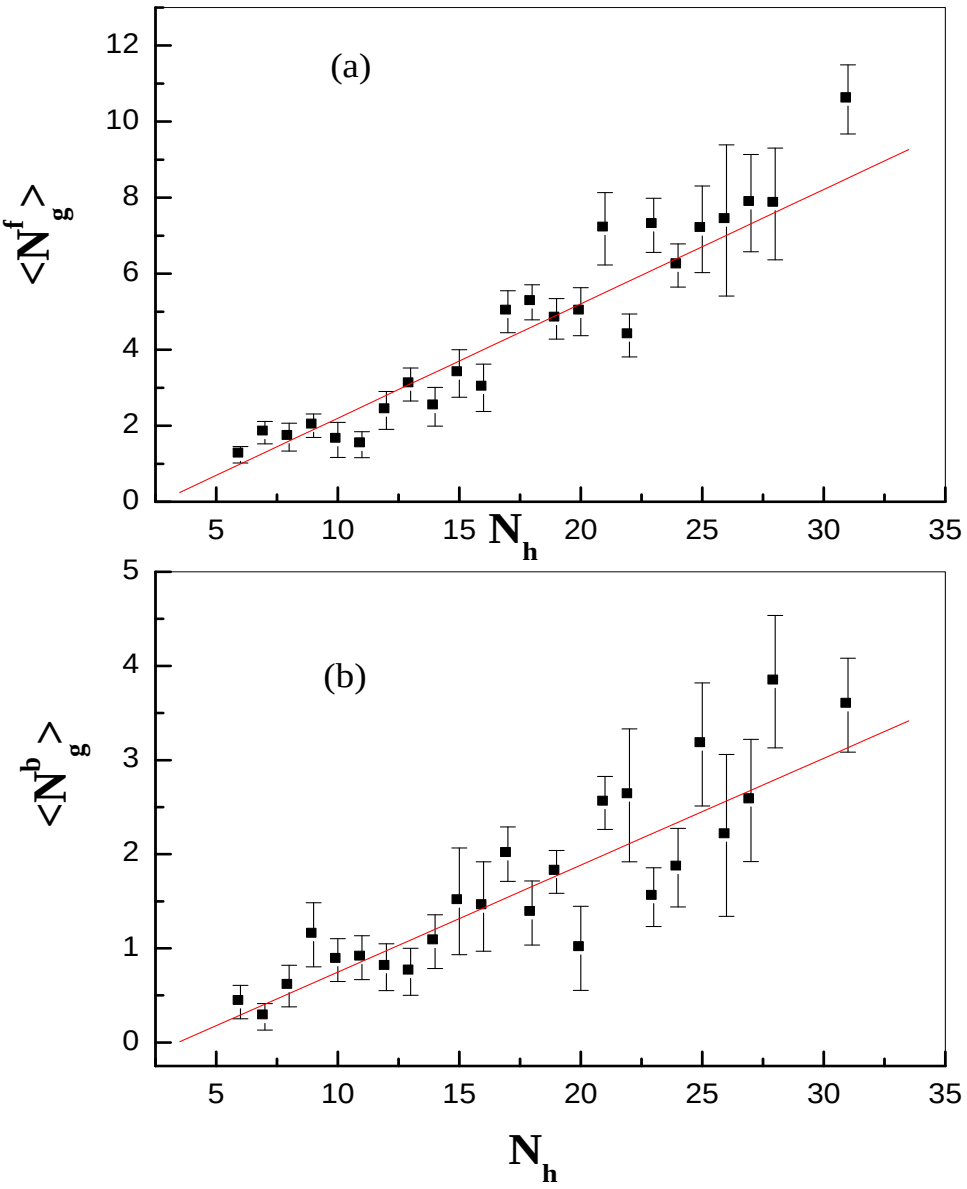

Fig. (III-9): *The dependence of the multiplicities of the grey particles (a) $< N^f_g >$ and (b) $< N^b_g >$ on the number of the target fragments N_h for the interaction of ^{28}Si at 14.6A GeV with emulsion nuclei together, with linear fitting of the experimental data.*

Now, the effect of the target size on the particles emitted in the latter stage of interaction in both the forward and backward hemisphere is discussed in Fig. (III-10).In this figure the dependence of the experimental average multiplicities of the black particles emitted in the forward hemisphere $< N_b^f >$ and that emitted in the backward hemisphere $< N_b^b >$ on (N_h) for the interaction of ^{28}Si at 14.6A GeV are displayed.

The Linear fitting of the experimental data is done over the range of (N_h) , in the dependence of$< N_b^f >$ on (N_h), while it is done over the whole range up to N_h =26 in the dependence of $< N_b^b >$ on (N_h).

From the figure, it can be deduced that,

- There is an increase of (N_h) values accompanied by a fast increase in the experimental average multiplicity of black particles emitted in the forward and backward hemisphere.
- The experimental values of$< N_b^f >$ are not much higher than those of $< N_b^b >$ over the whole range of (N_h).

All the fitting lines to the experimental points illustrated in the figures from fig. (III-9) through fig. (III-10) can be approximated by the following linear dependences with positive slopes,

$$< N_i^j > = A + B (N_h) \qquad \text{(III-10)}$$

Where A, B are the fitting parameters whose values are given in the table (III-12).

[i= g (grey), b (black)] and [j=f (forward), b (backward)]

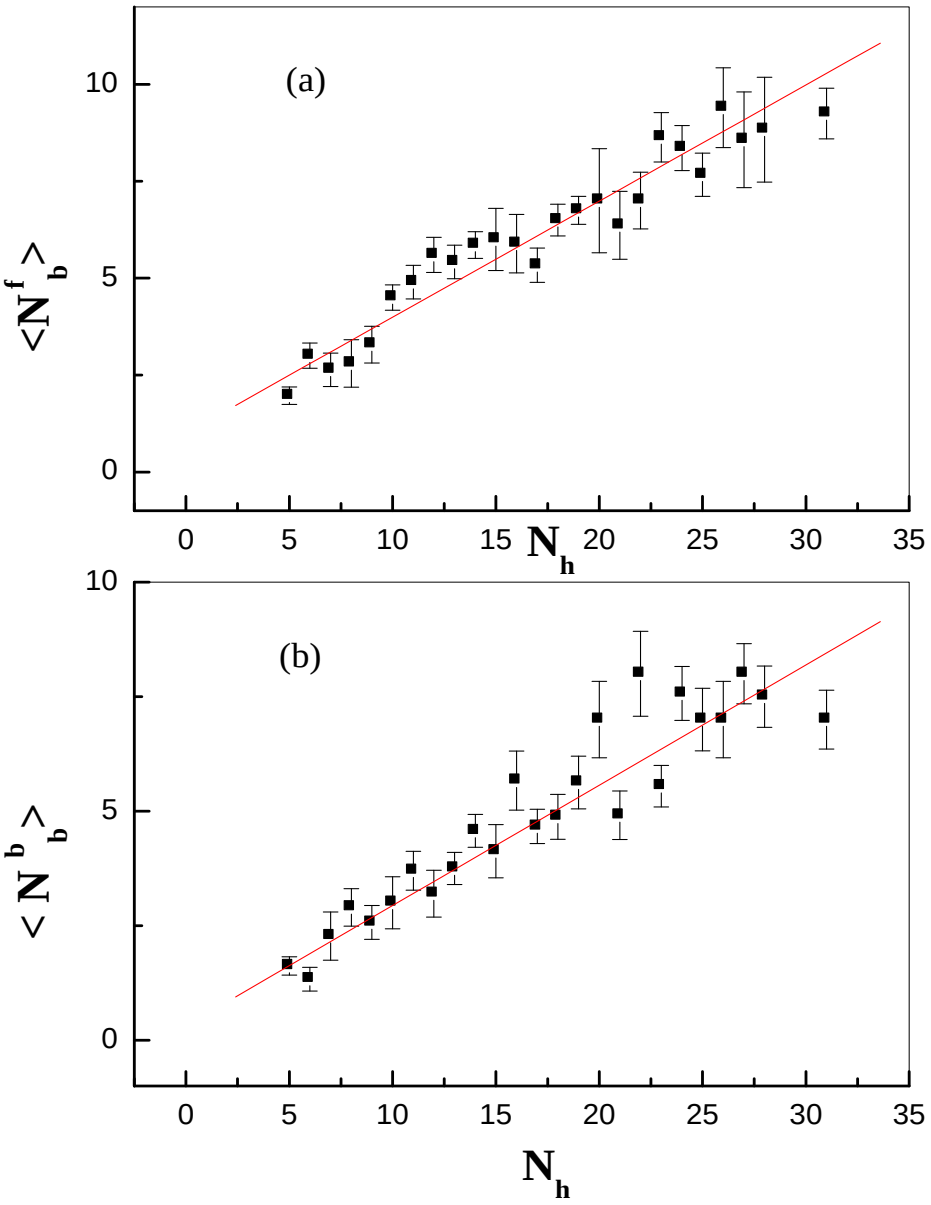

Fig. (III-10): *The dependence of the multiplicities of the black particles (a) $< N^f_b >$ and (b) $< N^b_b >$ on the number of heavily ionizing particles N_h for the interaction of ^{28}Si at 14.6A GeV with emulsion nuclei together, with linear fitting of the experimental data.*

Now fig. (III-11) displays the dependence of the forward emitted grey particles on the backward ones due to the interactions of ^{28}Si with emulsion nuclei at 14.6A GeV. From fig. (III-11), it is observed that,

The forward emitted grey particle multiplicity is correlated with the backward one in a linear relation of the form,

$$\left\langle N_g^f \right\rangle = A + BN_g^b \qquad \text{(III-11)}$$

A and B can be obtained by a linear fitting which is presented by the straight lines. The values of the parameters A and B are shown in Table (III-12).

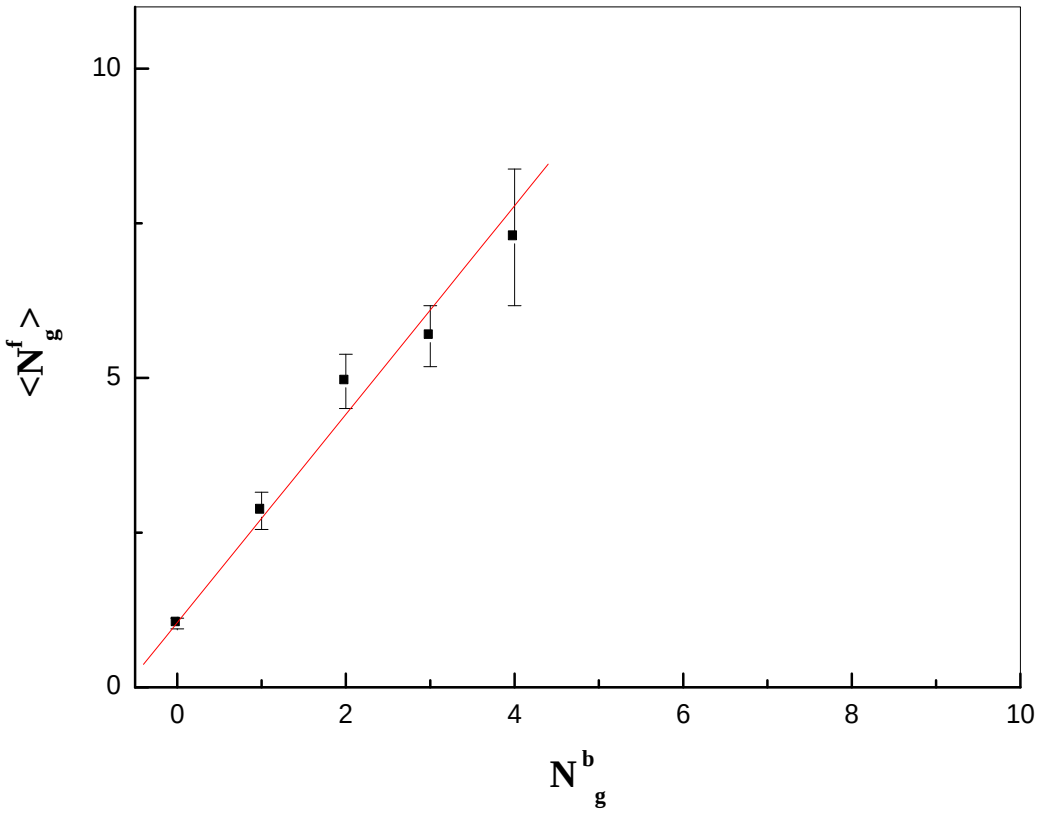

Fig. (III-11): *The correlation between the system emitting grey particles in FHS and BHS at high energy, together with the fitting presentation (straight lines).*

Now, the correlation between the system emitting black particles in FHS and that in BHS will be examined by displaying the dependence of $\langle N_b^f \rangle$ on N_b^b.

Fig. (III-12) shows the dependence of average black particles multiplicity $\langle N_b^f \rangle$ in FHS on the backward emitted black particles multiplicity N_b^b. From fig. (III-12) one can observe the strong dependence of $\langle N_b^f \rangle$ on N_b^b. Such dependence is presented by linear relation of the form,

$$\langle N_b^f \rangle = A + BN_b^b \qquad \text{(III-12)}$$

The correlation parameters A and B can be found from the fitting of the experimental data. The linear fitting is presented in fig. (III-12) by the straight lines. The values of the parameters A and B are given in Table (III-12).
Table (III-12) shows that,

1. The fitting parameters of $< N^f_g >$, $< N^b_g >$ have strong dependence on (N_h).
2. The fitting parameters of $< N_b^f >$, $< N_b^b >$ have strong dependence on (N_h).
3. The fitting parameters of $< N^f_g >$ have strong dependence on N^b_g.
4. The fitting parameters of $< N^f_b >$ have strong dependence on N_b^b

Therefore, one can conclude that, the system emitting grey and black particles in FHS is strongly correlated with that in BHS.

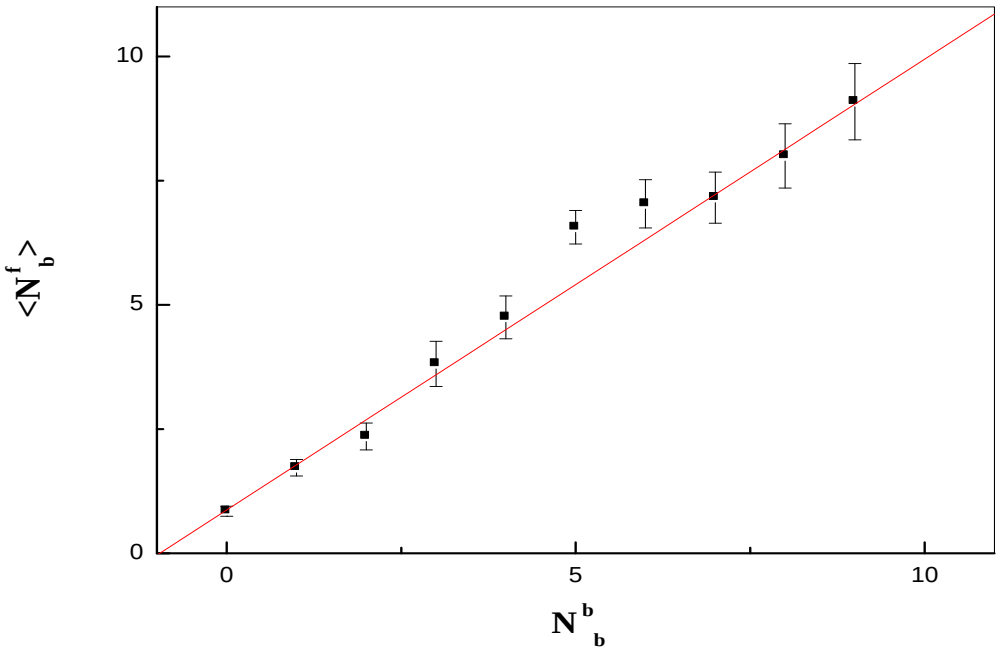

Fig. (III-12): *The correlation between the black particles in FHS and that in BHS, together with the fitting lines.*

Table (III-12): *The fitting parameters of the experimental data for the interactions of ^{28}Si at 14.6A GeV with emulsion* nuclei *belonging to the dependence of different average multiplicities on (N_h) and the correlation between the system emitting grey and black particles in FHS and that in BHS.*

Correlation	**Projectile**	
	^{28}Si (14.6 GeV)	
	A	**B**
$\langle N_g^f \rangle - N_h$	-0.81±0.30	0.30±0.02
$\langle N_g^b \rangle - N_h$	-0.38±0.15	0.12±0.01
$\langle N_b^f \rangle - N_h$	0.99±0.25	0.29±0.02
$\langle N_b^b \rangle - N_h$	0.32±0.23	0.26±0.02
$\langle N_g^f \rangle - N_g^b$	1.05±0.07	1.68±0.11
$\langle N_b^f \rangle - N_b^b$	0.87±0.18	0.91±0.07

(III-8)Angular Characteristics

(III-8.1.) Angular Characteristics of the Emitted Grey Particles:

The mean angle of the emitted grey particles $< \theta >_g$ in interactions of ^{28}Si– Em at 14.6A GeV is listed in table (III-13) and compared with the analogical data for different projectiles. Where $< \theta >_g$ is the medium angle (i.e. the angle at which half of the number of the specified particles are emitted).

One can find that, the value of the mean angle $< \theta >_g$ is nearly constant (i.e. independent of the projectile mass number). The angular distribution for grey particles emitted in the present interaction is shown in fig. (III-13). From this figure it can be noticed that, the distribution shows a peaking shape with peak positioned nearly at $\theta = < \theta >_g$. The number of the backward emitted particles (i.e. $\theta \geq 90^o$) decreases with increasing θ. The distribution of such backward angles follows an exponential decay. The angular distribution of grey particles can be reproduced successfully using the statistical model [27] and calculated according to the equation,

$$dN / d\theta_g \approx \sin\theta_g (F / B)_g^{\cos\theta_g} \qquad \text{(III-13)}$$

The predicted rational velocity **(** χ_o) according to statistical model will be given by the following equations**,**

$$\chi_o = \beta_{II} / \beta_o = \cos(< \theta >_g) \qquad \text{(III-14)}$$

So the values of the $\beta_{//}{}^g$, longitudinal velocity of the black particle emitting system can be deduced from the values of $\beta_o{}^g$ where,

$$\beta_{//}{}^g = \beta_o{}^g \chi_o{}^g \qquad \text{(III-15)}$$

Take [$\beta_o{}^g \approx 0.35$ from ref.(92)]

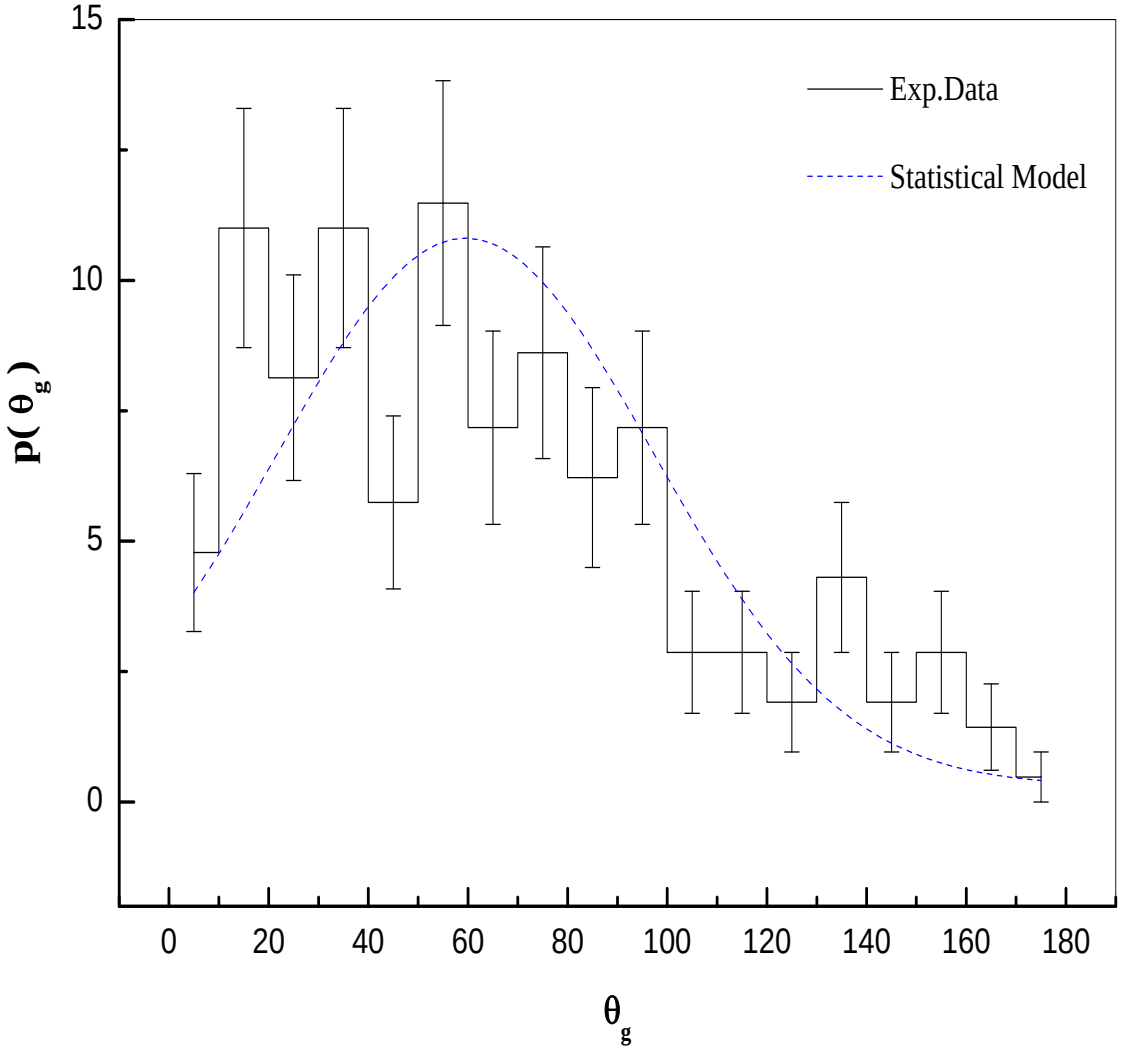

Fig. (III-13): *The angular distribution of grey particle emitted in the present interaction of ^{28}Si with nuclear emulsion at 14.6A GeV (histograms), together with the prediction of the statistical model and the Gaussian fitting shapes (smooth curves).*

Table (III-13): *The average values of the emission angles of the grey particles in different interactions at (2.2-14.6A GeV), in addition to the rational and longitudinal velocities of the system of grey particle emission, on the basis of statistical model.* [92, 94,102,103,104]

Projectile	Energy A GeV	$< \theta >_g$	χ_o^g	$\beta_{//}^g$	Ref
P	3.7	67.80 ± 1.20	0.37	0.13	92
^{4}He	3.7	62.80 ± 3.10	0.46	0.15	92
^{6}Li	3.7	64.90 ± 2.20	0.43	0.16	94
^{7}Li	2.2	63.50 ± 2.00	0.45	0.16	102
^{12}C	3.7	64.00 ± 1.90	0.44	0.15	92
^{22}Ne	3.3	63.70 ± 1.60	0.44	0.15	103
^{24}Mg	3.7	56.50 ± 4.50	0.55	0.19	104
^{28}Si	3.7	63.30 ± 1.44	0.45	0.16	103
^{28}Si	14.6	64.76 ± 2.06	0.43	0.15	Present Work

From Table (III-13) it is noticed that,

- The constancy in the values of $< \theta >_g \sim 64$, independent of the variation of projectile mass number as well as incident energy.
- The rational velocity for the system of grey particle emission $\chi_o{}^g$ is nearly equal 0.5 for different interactions studied here.
- The emitting system of the g- particles is fast and with typical longitudinal velocities $\beta_{//}{}^g \approx 0.13\text{-}0.20$

(III-8.2.) Angular Characteristics of the Emitted Black Particles

To investigate the angular characteristics for the system emitting black particles through the present 14.6A GeV ^{28}Si interactions with emulsion nuclei, the angular measurements are needed. The predicted distribution is presented in fig. (III-14) by dashed smooth curve. Regardless, the small shift of the solid curve to the left of the peak position of histogram, however one can say that the system responsible for the black particle emission is thermalized. The peaking shape is characterizing the angular spectrum. The spectrum seems to be symmetric about the peak position, which is near from the value of $\langle\theta_b\rangle$. The Gaussian distribution can approximate the angular spectrum successfully, to be presented by the dotted smooth curve. The feature of this spectrum implies that, the emission of black particles, in BHS and FHS, tends to be symmetric in both hemispheres, where the particle multiplicity increases in the vicinity region of $\theta_{lab} \sim 90^o$. The statistical model [27] reproduces the angular spectrum well by the equation,

$$dN / d\theta_b \approx \sin\theta_b (F/B)_b^{\cos\theta_b} \qquad \text{(III-16)}$$

The predicted rational velocity **(**χ_o) according to statistical model will be given by the following equations**,**

$$\chi_o = \beta_{II} / \beta_o = \cos(<\theta>_b) \qquad \text{(III-17)}$$

Which is the ratio of the longitudinal velocity of the center of mass, β_{II} to the characteristic spectral velocity, β_o of the fragmentation system. So the values of the $\beta_{//}{}^b$, longitudinal velocity of the black particle emitting system can be deduced from the values of $\beta_o{}^b$ where ,

$$\beta_{//}{}^b = \beta_o{}^b \chi_o{}^b \qquad \text{(III-18)}$$

Take $\beta_o{}^b \approx 0.115$ [from ref. (92)].Table (III-14) gives the average values of the emission angles of the black particles in different interactions in addition to the rational velocities of the system of black particle emission, on the basis of statistical model.

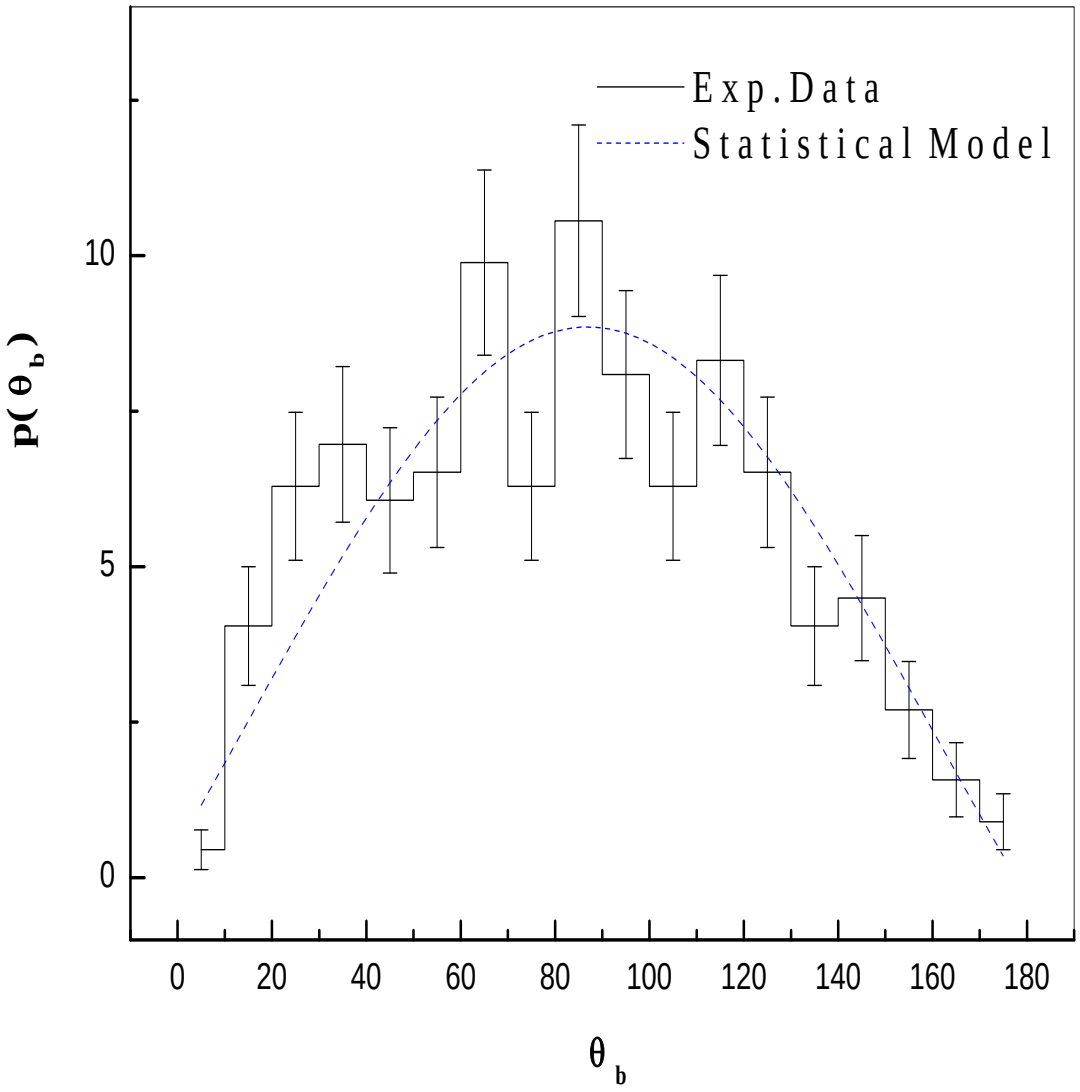

Fig. (III-14): *The angular distribution of black particle emitted in the present interaction of ^{28}Si with nuclear emulsion at 14.6A GeV (histograms), together with the prediction of the statistical model and the Gaussian fitting shapes (smooth curves).*

Table (III-14): *The average values of the emission angles of the black particles in different interactions at (3.7-14.6A GeV), in addition to the rational and longitudinal velocities of the system of black particle emission, on the basis of statistical model.* [92, 93, 97,104]

projectile	Incident Energy A GeV	$\langle\theta_b\rangle$	$\chi_o^{\ b}$	$\beta_{//}^{\ b}$	Ref
p	3.7	85.30±1.90	0.08	0.008	92
^{4}He	3.7	83.00±3.80	0.12	0.013	92
^{6}Li	3.7	82.20±2.60	0.14	0.015	97
^{7}Li	2.2	81.30±2.30	0.15	0.016	97
^{12}C	3.7	79.50±2.10	0.18	0.019	92
^{24}Mg	3.7	85.72±4.72	0.07	0.007	104
^{28}Si	3.7	83.3±1.18	0.12	0.013	93
^{28}Si	14.6	83.54±1.89	0.12	0.013	Present work

From Table (III-14) one can observe that,

- the constancy in the values of $\langle\theta_b\rangle \sim 80$, independent of the variation of projectile mass number as well as incident energy.
- The predicted rational velocity $\chi_o{}^{b}$ according to statistical model in section (I-8) tends to be ~ 0.13 for the system of black particle emission.
- The emitting system of the b- particles is slow and has a typical longitudinal velocities $\beta_{//}{}^{b}$ lie in the range $\beta_{//}{}^{b} \approx 0.008\text{-}0.019$

CONCLUSIONS

Conclusion

From studying the inelastic interactions of ^{28}Si ions with emulsion nuclei at incident energy 14.6A GeV, one can conclude the following:

1. The experimental mean free path λ_{exp}, for ^{28}Si ions in emulsion is 9.65 ± 0.42 cm. The value of λ_{exp} and the corresponding cross section value are close to those obtained in similar experiments. The experimental cross sectional values are in agreement with the empirical expectations of Bradt-Peters formula.

2. The interactions are categorized according to different emulsion target nuclei (H, CNO, and AgBr) into the following statistics:

- The interactions occurring with (H) are 56 events. The remaining 496 events are considered due to inelastic interaction with (CNO) and (AgBr) together.
- The group of events corresponding to the interactions with light nuclei (CNO) is 194 events.
- The group of events representing the interactions with AgBr nuclei is 302 events.

3. The multiplicity distributions of grey particles show no dependence on the incident energy, where the interactions of ^{28}Si with emulsion nuclei at 14.6A GeV have the same grey particles multiplicity distribution as that at 3.7A GeV.

4. The percentages of events accompanied by backward grey particles tend to be constant and dependent neither on the projectile size nor energy.

5. The grey particles emitted in FHS have multiplicity distributions of a similar behavior as those in BHS.

6. The strong dependence of the grey particles multiplicity on the target size is reflected on their average multiplicity which is larger for CNO than H, while for AgBr has the largest values.

7. It is clearly seen that the values of the decay parameters λ_g^b, characterizing the backward emitted grey particles multiplicity distributions, are nearly constant irrespective of the projectile size and energy. So the value of λ_g^b is completely independent on the projectile size and incident energy but decreasing with increasing target size. Consequently the probability of grey particle production in BHS increases with target size.

8. The values of forward to backward ratios, $(F/B)_g$, fluctuate about a constant value ~ 3.5, independent on the projectile size and incident energy. This observed constancy is regarded as a limiting behavior for the system of grey particles emission at relativistic energy. On the other hand the $(F/B)_g$ decreases with increasing target size.

9. The rational velocity for the system of grey particle emission, $\chi_o^{\mathbf{g}}$, is nearly equal to 0.5 for different interactions studied here.

10. The system of grey particle emission is fast and its typical longitudinal velocity, $(\beta_{//})^g$, has a range of ~ 0.13 to 0.22.

11. The normalized experimental distribution of black particles multiplicity for the interactions of ^{28}Si with emulsion nuclei at 14.6A GeV is nearly similar to that at 3.7A GeV within experimental errors. This behavior exhibits independence on the incident energy.

12. The percentages of events accompanied by backward black particles tend to be constant and dependent neither on the projectile size nor energy.

13. The black particles emitted in FHS have multiplicity distributions of a similar behavior as those in BHS.

14. The characteristic parameters of forward emitted black particles multiplicity distributions, α_b^f and λ_b^f, have nearly constant values which imply an independency on the projectile size and incident energy. The same trend is observed for the backward emitted black particles. Hence, the mechanism responsible for producing black particles in FHS may be similar to that in BHS.

15. The anisotropy ratio $(F/B)_b$ fluctuates about a constant value of ~ 1.4, independent on the projectile size or incident energy. The observed constancy, in the anisotropy ratios, indicates a limiting behavior for the system of black particles emission at relativistic energy.

16. The predicted rational velocity**,** $(\chi_o)^b$, for the system of black particle emission is found ~ 0.13.

17. The system of black particles emission is slow and its typical longitudinal velocities, $(\beta_{//})^b$, ~ 0.012 to 0.023.

18. The multiplicity dependency for the different emitted grey and black particles in both hemispheres can be approximated as a function of target size. The emission system of grey and black particles in FHS is strongly correlated with that in BHS by a linear relation.

19. The angular distributions of grey and black particles can be reproduced by Gaussian fitting shapes.

20. The average values of the emission angles for the grey and black particles always have constant values of $< \theta >_g$ ~ 64 and $< \theta >_b$ ~ 80, respectively for a wide domain of projectile mass numbers. This indicates independence on the projectile size and incident energy.

Finally one can say that, the backward emissions of fast (grey particles) and slow (black particles) protons are resulted from the decay of the system in a latter stage of the interaction and found to be dependent only on the target size (i.e. independent on projectile size or incident energy).

REFERENCES

References

[1] Meng Ta-chung, phys. Rev. Lett. **42**, 1331 (1979).

[2] J. Gosset, H. H. Gutbrod, W. G. Meyer, A. M. Poskanzer, A. Sandoval, R. Stock, and G. D. Westfall, Phys. Rev. **C16**, 629 (1977).

[3] I. A. Pshenichnov, I. N. Mishustin, J. P. Bondorf, A. S. Botvina, and A. S. Iljinov, Phys. Rev.**C27**, 1920 (1998).

[4] C. F. Powell, P. H. Flower, and D. M. Perkins, study of Elementary Particles by the Photographic Method (Pergamon, London, 1959).

[5]H. W. Barz, J. P. Bondorf, R. Donangelo, F. S. Hansen, B. Jakobsson, L. Karlsson, H. Nifenecker, R. Elme'r, H. Schulz, F. Schussler, K. Sneppen, and K. Soderstrom, Nucl. Phys. **A 548**, 427 (1992).

[6] F. Schussler, H. Nifenecker, B. Jakobsson, V. Kopljar, K. Soderstorm, S. Lerag, C. Ngo, Nucl. Phys. **A 584**, 704 (1995).

[7] H. H. Heckman, H. J. Crowford, D. E. Greiner, P. J. Lindstorm, and Lance W. Wilson, Phys. Rev. **C 17**, 1651 (1978).

[8] A. Abdelsalam, S. Voka'l, K. D. Tolstov, G. S. Shabratova, M. Sumbera, M. Haiduc, S. D. Bogdanov, V. I. Ostroumov, V. G. Bogdanov, V. A. Plyushchev, Z. I. Solovieva, and R. Togoo, Czech J. Phys. **B34**, 1196 (1984).

[9] M. S. Ahmad, M. Q. R. Khan, and R. Hasan, Nucl. Phys. **A 499**, 821 (1989).

[10] W. R. Webber, Proceedings of the international Cosmic Ray conference, vol. **8**, p. 65, Moscow, USSR (1987).

[11] J. P. Bondorf, A. S. Botvina, A. S. Iljinov, I. N. Mishustin, K. Sneppen, Physics Reports 275,133 (1995).

[12] J. P. Bondorf, Journal de Physique 37, C5-195 (1976).

[13] V. Lips et al., Phys. Rev. Lett. **72**, 1604 (1994).

[14] A. Dabrowska, R. Hotyn'ski, A. olszewski, M. Sza'rska, A. Trzupek, B. Wilczyn'ka, H. Wilczyn'ski, W. Wolter, B. Wosiek, K. Woz'naiak, Nucl. Phys.

A693, 777(2001).

[15] J. Hufner, K. Schafer, and B. Shurman, Phys. Rev. **C12**, 1888 (1985).

[16] K. Summerer, W. Bruchle, D. J. Morrissey, M. Schadel, B. Szweryn, and Yang Weifan, Phys. Rev. **C42**, 2546 (1990).

[17] A. Abdelsalam, Physica-Scripta. Vol **47**, 505-511(1993).

[18] S. Nagamiya et al., Phys. Rev. **C24**, 971(1981) and references therein.

[19] A. M. Baldin et al., Sov. J. Nucl. Phys. **20**, 629(1976); Proceedings of the 6th International Conference on High Energy Phys. and Nucl. Structure edited by D. E. Nagle and A. S. Goldhaber, 620 (AIP, New York, 1975).

[20] A. Abdelsalam, B. M. Badawy, and E. El–Falaky, Canadian Journal of Physics **85**, 837-848 (2007).

[21] P. Freier, E. J. Lofgren, E. P. Ney, F. Oppen heimer, H. L. Bradt and B. Peters, Phys.Rev. **74**, 213 (1948).

[22] H. H. Heckman, Lawrence Berkely Laboratory Report LBL 2052 (1973).

[23] A. M. Baldin, Joint Institute for Nuclear Research Report E–9138 (1975).

[24] Florian J P et al. Report submitted to the meeting of Division of particles and fields, (Berely).

[25] A.Abdelsalam JINR Report (Dubna) El-81-623(1981).

[26] A. Abdelsalam, E. A. Shaat, N. Ali Mossa, Z. Abou-Moussa, O. M. Osman, N. Rashed, W.Osman, B. M. Badawy, and E. El-Falaky,Journal of Physics G **28**, 1375 (2002).

[27] H. H. Heckman, H. J. Crowford, D. E. Greiner, P. J. Lindstorm, and Lance W. Wlson, phys. Rev. **C 17**, 1651 (1978).

[28] B. M. Badawy, Int. J. Mod. Phys. **E 18**, 643 (2009).

[29] Sarkar, S., Satz, H., Sinha, B. (Eds.), "The Physics of the Quark-Gluon Plasma Introductory, Lectures", Lect. Notes Phys. 785, 46 (Springer, Berlin Heidelberg (2010).

[30] J.C.Hill et al., Phys.Rev.Lett. **60**,999(1988).

[31] D.L.Olson et al., Phys.Rev. **C24**, 1529(1981).

[32] G. Baur and C. A. Bertulani, Phys. Rev. **C34**, 1654 (1986).

[33] G. A. Bertulani and G. Baur, Phys. Rev. **163**, 299 (1988).

[34] H. L. Bradt and B. Peters, Phys. Rev. **77**, 54 (1950).

[35] H. L. Bradt and B. Peters, Phys. Rev. **80**, 943 (1950).

[36] F. Schussler, H. Nifenecker, B. Jakobsson, V. Kopljar, K. Soderstorm, S. Lerag, C. Ngo, Nucl. Phys. A 584, 704 (1995).

[37] A.Abdelsalam JINR Report (Dubna) **El-**81-623(1981).

[38] A. Abdelsalam, E. A. Shaat, N. Ali Mossa, Z. Abou-Moussa, O. M. Osman, N. Rashed, W.Osman, B. M. Badawy, and E. El-Falaky,Journal of Physics G **28**, 1375 (2002).

[39] P. L. Jain, K. sengupta and G. singh, Phys. Rev. Lett **59**, 2531 (1987).

[40] M. I. Adamovich et al, Eur Phys. J **A1**, 77 (1998).

[41] B. M. Badawy, Int. J. Mod. Phys. E **18**, 643 (2009).

[42] A. Abdelsalam, B. M. Badawy, and E. El–Falaky, Canadian Journal of Physics **85**, 837-848 (2007).

[43] V.S.Barashenkov and V.D.Toneev, Interactions of High Energy Particles and Atomic Nuclei with Nuclei, Moskva, Adomizdat, 12(1972), (in Russian).

[44] R.J.Glauber, "Lectures in Theoretical Physics", (Wiley–Interscience, New York), Vol.**I**, 315(1959).

[45] M.K.Hegab, M.T.Hussien and N.M.Hassn, Z.Phys**. A336**, 345(1990) and references therein.

[46] W.Czyz and L.C.Maximon, Ann.Phys.(New York)52, 59(1969).

[47] A.P.Gasparyan et al., JINR Report 1–12797, Dubna, (1979).

[48] H.L.Bradt and B.Peters, Phys. Rev. **77**, 54 (1950); **80,** 943 (1950); T.F.cleghorn, F.S.Freier and C.J Waddington, Can. J. Phys. **46**, S 572 (1968).

[49] M.I.Adamovich et al., cosmic and subatomic Phys. Report. Lund univ. Luip 8904 and Luip 8907 (1989).

[50] K. K. Gudima, V. D. Toneev, Preprint JINR, E P2–1043, Dubna (1977).

[51] A. Abdelsalam, M. Šumbera and S. Vokál, JINR, El–82–509 (Dubna, 1982) and Int. Conf. on Nucl.–Nucl. Interactions, (Michigan, 1982).

[52] N. Ali–Moussa, Arab. Journal of Nuclear Sciences and Applications, **33**

(1), 211 (2000).

[53] S. Nagamiya et al., Phys. Rev. **C24**, 971(1981) and references therein.

[54] S. Frankel, Phys. Rev. Lett. **38**, 1338 (1977).

[55] R. D. Amado and R. M. Wloshyn, Phys. Rev. Lett. **36**, 1435 (1976).

[56] R. D. Amado and R. M. Woloshyn, Phys. Lett. **69B**, 400 (1977).

[57] T. Fujita, Phys. Rev. Lett. **39**, 174 (1977).

[58] L. S. Schroeder, Berkeley Preprint–LBL 11102, Nuclear Studies, Kikuchi Summer School on Nuclear Physics at High Energies, Fuji–Yoshida, Japan, July 1–4, (1980) and references therein.

[59] Yu. D. Bayukov et al., Phys. Rev. **C20**, 764 (1979).

[60] M. L. Perl, High Energy Hadron Physics, John Wiley and Sons, New York, 201 (1974).

[61] T. Fujita and J.Hüfner, Nucl. Phys. **A314**, 317 (1979) and references therein.

[62] T. Fujita, Nucl. Phys. **A324**, 409 (1979).

[63] L. L. Frankfurt and M. I. Strikman, Phys. Lett. **B83**, 497 (1979).

[64] T. Yukawa and S. Furui, Phys. Rev. **C20**, 2316 (1979).

[65] L. S. Schroeder, Berkeley Preprint–LBL 11102, Nuclear Studies, Kikuchi Summer School on Nuclear Physics at High Energies, Fuji–Yoshida, Japan, July 1–4, (1980) and references therein.

[66] L. S. Schroeder, Nucl. Inst. and Meth. **162**, 385 (1979).

[67] S. Frankel, Phys. Rev. Lett. **38**, 1338 (1977).

[68] J. W. Harris, Proceeding of the Workshop on Nuclear Dynamics 80 (California–March 1980).

[69] N. A. Burgov et al., Sov. J. Nucl. Phys. **24**, 620 (1976).

[70] EMUO1 Collaboration: M. I .Adomvich et al., Phys. Lett. **B234**, 180 (1990).

[71] A. M. Baldin et al., Yad. Fiz., 20, 1201(1975)[Sov. J. Nucl. Phys. **20 (6)**, 629 (1975)].

[72] C. F. Perdrisat, S. Frankel and W. Frati, Phys. Rev. **C18**, 1764 (1978).

[73] J.Papp et al., Phys.Rev.Lett. **34**, 601(1975).

[74] V. V. Burov , V. K. Lukyanov and A. I. Titov, Phys. Lett. **67B**, 46 (1977).

[75] I. A. Schmidt and R. Blankenbecler, Phys. Rev. **D15**, 3321 (1977).

[76] Meng Ta–Chung, in Proceedings of the Symposium on Relativistic Heavy Ion Collisions, 1978, edited by R.Bock and R.Stock (Gesellschaft für Schwerionen–Forchun, Darmstadt, W. Germany, 1978).

[77] A. M. Baldin, in Proceedings of the 19th International Conference on High Energy Physics, Tokyo, Japan, 1978.

[78] H. B. Mathis and Meng Ta–Chung, Phys. Rev. **C18**, 952 (1978), and references therein.

[79] Dipak Gosh et al., Z.Phys. **A342**, 191(1992).

[80] Dipak Gosh and Ranjan Senpupta, Nucl.Phys. **A470**, 683 (1987).

[81] CERN European Organization for Nuclear Research, CERN 63-3,225(1963).

[82] W.H.Barkas, Nuclear Research Emulsion, New York Academic press, **1**st Ed., **49**(1963).

[83] H. L. Bradt and B. Peters, Phys. Rev. 77, 54 (1950); 80, 943 (1950); T. F. cleghorn, F. S. Freier and C. J Waddington, Can. J. Phys. **46**, S 572 (1968).

[84] A. Abdelsalam, M. S. El-Nagdy, E. A. Shaat, N. Ali-Moussa,O. M. Osman, Z. Abou-Moussa, S. Kamel, N. Rashed, W. Osman, M. E. Hafiz, B. M. Badwy, and S. Magd Eldin, FIZIKA **B 15**,9 (2006).

[85] M. A. Jilany, Nucl. Phys. **A 579**, 627 (1994).

[86] B. P. Bannik et al., Sov. J. Nucl. Phys. **52**,982 (1984).

[87] A. Abdelsalam, M. S. El–Nagdy, N. Rashed, B. M. Badawy, and E. El–Falaky, Journal of Nuclear and Radiation Physics **2**, 49 (2007).

[88] M. El–Nadi, A. Abdelsalam, N. Ali Mossa, Z. Abou–Moussa, S. Kamel, Kh. Abdel–Waged, W. Osman, and B. M. Badawy, The European Physical

Journal **A 3**, 183 (1998).

[89] S. El-Sharkawy, M. K. Hegab, O. M. Osman and M. A. Jilany, Physica Scripta **47**, 512 (1993).

[90] M. El-Nadi et al., IL Nuovo Cimento **A 108**, 831 (1995).

[91] M. El-Nadi, A. Abdelsalam, N. Ali-Moussa, Z. Abou-Moussa, Kh. Abdel-Waged, W. Osman, and Badawy, IL Nuovo Cimento **A 111**, 1243 (1998).

[92] A.Abdelsalam, Phys. Scr., **47,** 124 (1993).

[93] Mennatallah. M. M., M.Sc. Thesis submitted to Faculty of Science, Cairo University (2011) and references therein.

[94] M.I.Adamovich; et al. LUND Report LUIP 8906 (1989).

[95] Noha. A. Abdelsalam, M. Sc. Thesis submitted to Faculty of Education, Ain Shams University (2012) and references therein.

[96] M. El–Nadi, A. Abdelsalam, N. Ali–Mossa, Z. Abou–Moussa, S. Kamel, Kh. Abdel–Waged, W. Osman, and B. M. Badawy, Eur. Phys. J. **A 3**, 183 (1998).

[97] M. El-Nadi, A. Abdelsalam, N. Ali-Moussa, Z. Abou-Moussa, Kh. Abdel-Waged, W. Osman, and Badawy, IL Nuovo Cimento **A111**, 1243 (1998).

[98] A. Abdelsalam, B. M. Badawy, and E. El–Falaky, Canadian Journal of Physics **85**, 837-848 (2007).

[99] A. Abdelsalam, E. A. Shaat, N. Ali Mossa, Z. Abou–Moussa, O. M. Osman, N. Rashed, W. Osman, B. M. Badawy, and E. El–Falaky, Journal of Physics **G 28**, 1375 (2002).

[100] M. El-Nady, A. Abdelsalam, and N.Ali-Moussa, Int. J. Mod. Phys.F.,**3**,811,(1994); Radi.Phys.Chem. **47**,681(1996); IL Nuovo Cimento **A,110**, 1255 (1998).

[101] LI Hui-Ling, ZHANG Dong-Hai, and LI Jun-Sheng, Chinese Journal of Physics C (HEP&NP) Vol.**33**:521-558(2009).

[102] M. El-Nadi, et al., Il Nuovo Cimento Vol. **107A.** N. 1 Gennaio (1994).

[103] M.M.Sherif, Il Nuovo Cimento Vol. **109A**, 1135 (1996).

[104] Z. A. Soliman, Ph. D. Thesis submitted to Faculty of Science, Cairo University (2010) and references therein.

ARABIC ABSTRACT

الملخص العربي للرسالة

تتناول هذه الرسالة تحليل عملية إنتاج الهادرونات السريعة و البطيئة من خلال التفاعلات غير المرنة لأنوية السيليكون (28) مع أنوية المستحلب النووي عند طاقة 14.6 جيجا إلكترون فولت لكل نيوكليون ، وذلك بالبحث عن البارامترات المؤثرة والآليات المسئولة عن إنتاجية تلك الهادرونات.

تم دراسة التوزيع العددي للجسيمات المتأينة الثقيلة و مقارنتها بمثيلاتها لتفاعل أنوية السليكون عند طاقة 3.7جيجا الكترون فولت.و في هذه الدراسة وجد أن لا يعتمد على حجم نواة المقذوف .

كما تم دراسة عملية فصل الأحداث الإحصائية إلى مجموعات وفقا لنواة الهدف بطرق مختلفة منها طريقة فلوريان ، هذه الطريقة تعتمد أساسآ على عدد الجسيمات المتأينة. ومن خلال تلك الطرق المتاحة للفصل بين انوية المستحلب النووي فقد أمكن تصنيف التفاعلات حسب حجم أنوية المستحلب وفي محاولة لفهم ديناميكية تشظي نواة الهدف الي جسيمات رمادية وسوداء، فقد تم دراسة التوزيعات العددية للجسيمات الرمادية والسوداء في الاتجاه الأمامي والخلفي ووجد أنها ذات مظهر أضمحلالي. كماوجد أنه بينما يعتمد ثابت الأضمحلال على حجم نواة الهدف فإنه لا يعتمد على حجم نواة المقذوف.

كما تم دراسة النسبة المئوية لعدد التفاعلات المصاحبة للجسيمات السريعة والبطيئة الخلفية ومقارنتها بتفاعلات أنوية اخرى ووجد أنها نسبة ثابتة ولا تعتمد علي حجم نواة المقذوف ولا الطاقةالساقطة.

كما تم دراسة تأثير حجم نواة المقذوف على خصائص التوزيع العددي للهادرونات المنبعثة في الأتجاه الأمامي والخلفي و مقارنتها بمثيلاتها لتفاعل أنوية السليكون عند طاقة 3.7جيجا الكترون فولت و في هذه الدراسة وجد أن إنبعاث الهادرونات في الإتجاه الأمامي و الإتجاه الخلفي لاتعتمد في سلوكها علي الطاقة الساقطة.

وتم دراسة النسبة بين القيم المتوسطة للجسيمات السريعةوالبطيئة الأمامية والخلفية ومقارنتها بتفاعلات أنوية أخرى عند طاقات مختلفة ووجد أنها نسبة ثابتة ولا تعتمد علي حجم نواة المقذوف ولا الطاقةالساقطة.

وقد أظهرت هذه الدراسة مدي الارتباط بين عدد ا لهادرونات المنبعثة في الإتجاه الأمامي و الخلفي وبين عدد الجسيمات المتأينة الثقيلة .

كما وجد ارتباط وثيق بين عدد ا لهادرونات المنبعثة في الإتجاه الأمامي وبين عدد ا لهادرونات المنبعثة في الإتجاه الخلفي ممثلا ذلك بعلاقة خطية.

وبناءاً على احصائية ماكسويل – بولتزمان تم تعديل النموذج الديناميكي الحراري والذي نجح في توقع الخصائص الزاوية للمنظومات المنبعث منها الهادروات السريعة والبطيئة . كما تم تحليل التوزيع الزاوي للهادرونات للعينة الكلية ، وفق معايير معينة وتم تمثيلها بنموذج جاوس ووجد أن القيمة المتوسطة لزاوية الانبعاث لكلاً من الهادرونات السريعة والبطيئة لاتعتمد علي حجم نواة الهدف كما لا تعتمد علي الطاقة الساقطة .


الله
جل جلاله

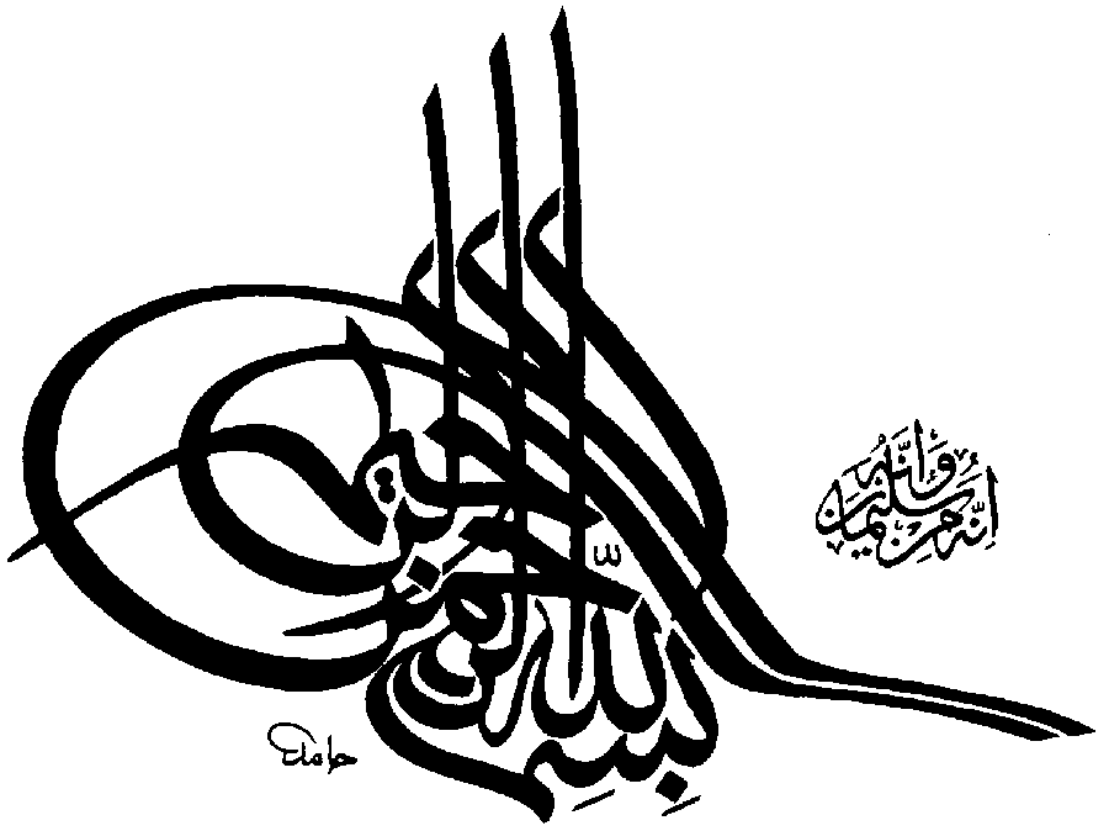
بسم الله الرحمن الرحيم
إنه من سليمان وإنه
حامد

جا معة بنـها
كلية الهندسة بشبرا
قسم الرياضيات والفيزيقا الهندسية

دراسة الجسيمات المختلفة الناتجة من تفاعل الأنوية الثقيلة مع أنوية المستحلبات النووية عند الطاقات العالية

رساله مقدمة إلى
جا معة بنـها- كلية الهندسة بشبرا
قسم الرياضيات والفيزيقا الهندسية

مقدمة من

مهندس
عبدالناصر صابر عبدالفتاح سليمان

بكالوريوس فى الهندسة الكهربية (قوى وألات كهربية)
كلية الهندسة بشبرا - جامعة بنـها (2005)
معيد بقسم الرياضيات والفيزيقا الهندسية - كلية الهندسة بشبرا- جامعة بنـها

للحصول على
درجة الماجستير فى الفيزياء الهندسية

تحت إشراف

أ.د/ عبدالله عبدالسلام محمد
أستاذ الفيزياء النووية
كلية العلوم- جامعة القاهرة

أ.د/ محمد السيد النجدي
أستاذ الفيزياء النووية
كلية العلوم- جامعة حلوان

أ.م.د / أحمد محمد عبدالله
أستاذ الفيزياء الهندسية المساعد
كلية الهندسة بشبرا– جامعة بنها

كلية الهندسة بشبرا - جامعة بنها

2012